NOAA Technical Memorandum OAR GSL-76
https://doi.org/10.25923/937j-s495

Diagnostic fields for hourly updated NOAA weather models - RRFSv1, HRRRv4, RAPv5

Stanley G. Benjamin[1,2], Eric P. James[1], Jaymes S. Kenyon[1,2],
Benjamin Blake[3], David D. Turner[1]

[1]NOAA Global Systems Laboratory, Boulder, CO
[2]Cooperative Institute for Research in Environmental Sciences, University of Colorado, Boulder, CO
[3]NOAA National Weather Service, NCEP, Environmental Modeling Center, College Park, MD

15 January 2026

Abstract

This document describes methods for diagnosing non-prognostic variables from explicit prognostic variables from hourly updated NOAA models from 2020 onward. A previous diagnostics technical memorandum (Benjamin et al. 2021a) described diagnostics for earlier versions of the hourly updated models. Here, we describe diagnostics applicable to the **High-Resolution Rapid Refresh (HRRRv4)** and **Rapid Refresh (RAPv5)** models implemented in December 2020 and to the **Rapid Refresh Forecast System (RRFS)** starting in 2026. The code for these diagnostics resides primarily within the Unified Post-Processor (Unipost or UPP) program used for common NOAA NCEP modeling system output.

Table of Contents

1. Introduction

This document describes diagnostic output fields for the closely related NOAA Rapid Refresh (RAPv5), the High-Resolution Rapid Refresh (HRRRv4) and the Rapid Refresh Forecast System (RRFSv1) hourly updated weather models. These descriptions provide at least general information on the diagnostic techniques by which these fields are calculated but do not include code-level details. The diagnostic fields described do not include *all* output fields from the RAP, HRRR and RRFS but only those for which the diagnostic method was not obvious and description is needed for interpreting the fields by forecast users. For diagnostic techniques relevant to earlier versions of the HRRR (v1-v3) and RAP (v1-4), see Benjamin et al. (2021a).

The RAP, with 13-km grid spacing, was implemented at NOAA/NCEP in 2012 (Benjamin et al. 2016a). The HRRR (Dowell et al. 2022, James et al. 2022), with 3-km grid spacing and explicit convection, was implemented at NCEP in 2014, but also ran experimentally at NOAA GSD since 2009. Many of the diagnostic techniques used in RRFSv1, HRRRv4, and RAPv5 explained in this document were developed initially for use in the hourly updated Rapid Update Cycle (RUC, Benjamin et al. 2004) model run at NCEP from 1998-2012. Table 1 provides a history of the versions of the RUC, RAP, HRRR, and future RRFS models to clarify changes made to these diagnostics at certain points in code history.

Both the RAP and HRRR models use the common NCEP post-processing program, Unipost (also known as the Unified Post-Processor - UPP, github UPP code), which has been used for approximately the last decade for all NCEP models. The diagnostics described in this document are generated either in the UPP code or directly diagnosed within the forecast model (WRF-ARW for RAP and HRRR). These diagnostic methods have been carried over for output fields from the Rapid Refresh Forecast System (RRFS) model (Carley et al 2023), which is part of the Unified Forecast System. RRFSv1 (FV3 used for forecast model dynamic core instead of WRF-ARW used for HRRR/RAP) is currently planned for operational implementation at NCEP in 2026. HRRR and RAP will continue to be run operationally at NCEP until RRFSv2 implementation, currently scheduled for 2028-2029.

Graphical examples are shown in this memo for many diagnostic fields. All fields are stored in GRIB2 using SI (International System of Units) / metric units even though some graphics are displayed using conversion to non-SI units (e.g., knots, degrees Fahrenheit).

HRRR GRIB2 Inventories :
Two-dimensional fields. Native hybrid model level fields. Isobaric level fields. Sub-hourly fields.
RAP GRIB2 Inventories : Two-dimensional fields. Native hybrid model level fields. Isobaric level fields.
RRFSv1 GRIB2 Inventories: (viewable with non-Chrome browsers)
Native model level fields Isobaric-level fields Sub-hourly fields

Table 1. History of rapidly updated model and assimilation systems at NCEP (as of 2026). Dates for implementation for experimental versions at NOAA ESRL/GSD/GSL are also shown. **RUC** = Rapid Update Cycle. **RAP** = Rapid Refresh. **HRRR** = High-Resolution Rapid Refresh. Experimental output from the RAPv5 and HRRRv4 models before their implementation in Dec 2020 are labeled in some figures in this document as RAPX and HRRRX, respectively. **RRFS** = Rapid Refresh Forecast System.

Model and assimilation system	**Horizontal grid spacing**	**Number of vertical levels**	**Assim. frequency**	**Implementation (month/year)**		**Geographical domain**
				NCEP	**ESRL/ GSL**	
RUC1	60 km	25	3h	**1994**		CONUS
RUC2	40 km	40	1h	**4/1998**		CONUS
RUC20	20 km	50	1h	**2/2002**		CONUS
RUC13	13 km	50	1h	**5/2005**		CONUS
RAP v1	13 km	51	1h	**5/2012**	**2010**	N. America
RAP v2	13 km	51	1h	**2/2014**	**1/2013**	N. America
RAP v3	13 km	51	1h	**8/2016**	**1/2015**	N. America
RAP v4	13km	51	1h	**7/2018**	**5/2017**	N. America
RAP v5	13km	51	1h	**12/2020**	**5/2019**	N. America
HRRR	3 km	51	1h	**9/2014**	**2010**	CONUS
HRRR v2	3 km	51	1h	**8/2016**	**4/2015**	CONUS
HRRR v3	3 km	51	1h	**7/2018**	**5/2017**	CONUS, Alaska
HRRR v4	3 km	51	1h	**12/2020**	**6/2019**	CONUS, Alaska
RRFS v1	3 km	65	1h	**Estim. 4/2026**	**4/2025 (exp at NCEP)**	N. America

Some of the diagnostic differences between HRRRv4 and RRFSv1 described in this document are related to differences in the data assimilation and model configurations. In Table 2, we summarize the common points and differences in these configurations. For instance, RRFSv1 uses a convective parameterization but HRRRv4 does not. RRFSv1 uses a full ensemble control member for its initialization whereas HRRRv4 uses an ensemble mean with a drying effect as noted by Benjamin et al. (2025). There is a very substantial difference, of course, in the dynamic core for the forecast model with RRFSv1 using the FV3 core (Carley et al. 2023) compared to HRRRv4 using the WRF-ARW core (Dowell et al. 2022).

There are many similarities between RRFSv1 and HRRRv4, with RRFSv1 maintaining assimilation features including a non-variational stratiform cloud analysis (Benjamin et al 2021b), coupling with the Great Lakes FVCOM model (Fujisaki-Manome et al 2020), and the addition of a 1-d lake model to represent variations in lake surface temperatures for smaller inland lakes (Trahan et al. 2025, Benjamin et al. 2022b). RRFSv1 also carries most of the same model parameterizations used in HRRR but with updated versions, e.g., for turbulence (MYNN, Olson et al. 2026), cloud microphysics (Thompson) and land-surface models (RUC LSM, Smirnova and Benjamin 2025). Gravity-wave drag (GWD, Toy et al. 2025) is also applied in both RRFSv1 and HRRRv4.

Table 2. RRFSv1 vs. HRRRv4 for model and data assimilation components

Data assimilation

	RRFSv1	HRRRv4	References
Overall	Ens control analysis	Ensemble mean	Dowell et al 2022, Fig. 3
Cloud DA	Yes	Yes	Benjamin et al 2021b
Soil DA	Yes	Yes	Benjamin et al 2022a
Lake cycle	Yes	Yes	Benj et al 2022b, Trahan et al 2025
FVCOM coupled	Yes	Yes	Fujisaki-Manome et al 2020
2m Td diagnosis (effect on assimilation)	Linear	Flux	This document

Model

	RRFSv1	HRRRv4	References
Dycore	FV3	WRF-ARW	Carley et al 2023, Dowell et al 2022
Convective cloud	Aligo-scale-aware SAS	none	
Turbulence	MYNN-2022	MYNNv3.8	Olson et al 2019, 2026
Subgrid-scale clouds	MYNN-2022	MYNNv3.8	Olson et al 2019, 2026
Cloud microphysics	Thomp-Eid 2022 version	Thomp-Eid 2014	Thompson and Eidhammer 2014
Land-surface model	RUC LSM	RUC LSM	Smirnova and Benjamin 2025
Gravity-wave drag	Yes	Yes	Toy et al 2025

2. Descriptions of diagnostics by category

Diagnostic fields are grouped by variable type, each with a summary of the method.

A. Humidity-related variables

i. Relative humidity

Relative humidity (RH) is always defined for output from the hourly updated models using *saturation with respect to water* (i.e., over a plane surface of liquid water) at all levels regardless of air temperature for RAP/HRRR and RRFSv1 isobaric fields and in the 2-m RH field. This approach was also used for the NOAA NAM weather model. In contrast, GFS output fields (up through GFSv16) calculate RH using a different saturation vapor pressure definition partially with respect to ice at cold temperatures up through GFSv16. GFSv17 (planned for late 2026) will switch to the same RH definition used by HRRR, RAP, RRFSv1, and NAM. Examples are shown for 850-hPa RH, and 850-500-hPa mean RH graphics (see Figs. 1-2).

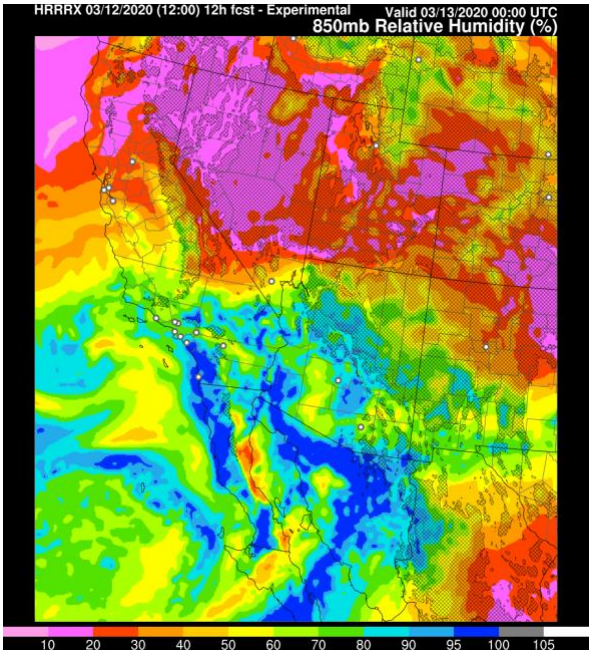

Fig. 1: Mean RH for 850-hPa layer. From 12-h HRRRv4 forecast valid at 00 UTC 13 Mar 2020. Note that regions where the ground is at a lower pressure than 850 hPa are shown as hatched.

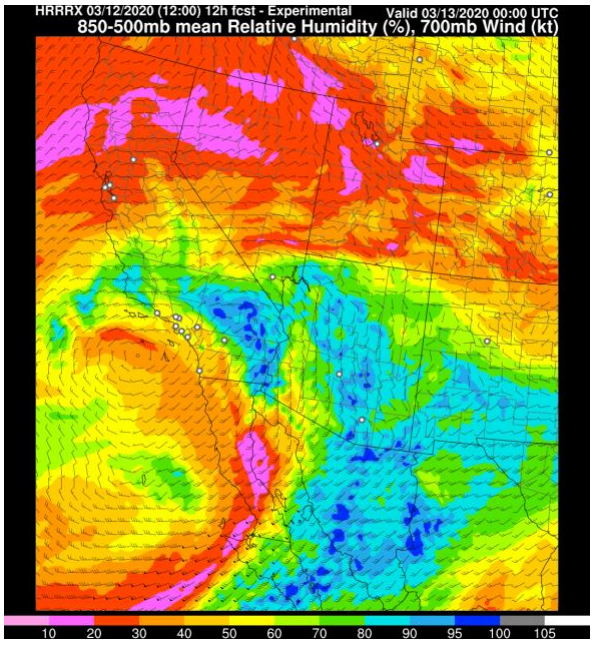

Fig. 2: 850-500-hPa RH. From 12-h HRRRv4 (labeled HRRRX) forecast valid at 00 UTC 13 Mar 2020. The RH fields show deep moisture surging northward into the southwestern CONUS associated with an approaching upper-level low.

ii. Precipitable water

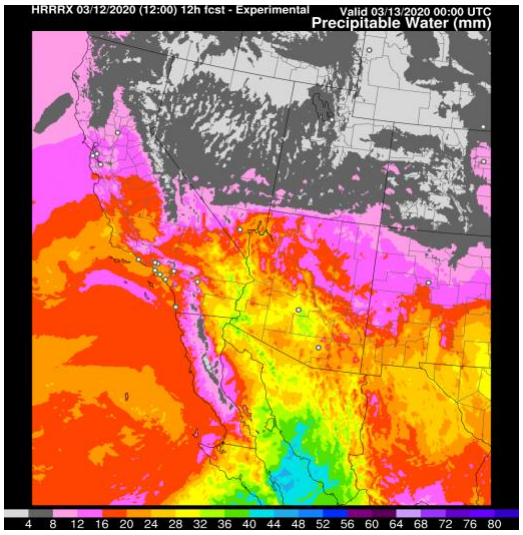

Precipitable water (PW), which is the vertically integrated water vapor in a column (Fig. 3), is defined in a manner consistent with meteorological convention, where water-vapor specific humidity at each vertical level is multiplied by the vertical pressure thickness of the layer surrounding that level (with other factors), and then summed over the model atmosphere from the model surface (ground) to the model top (10 hPa for RAP, 15 hPa for HRRR, 2 hPa for RRFSv1). This diagnosed PW is relative to the model surface elevation at a given gridpoint, so this field will usually show topographically related variations as in the example below over ridges in the state of Nevada and also over the Sierra Nevada mountains in California and Baja.

Fig. 3. Precipitable water. From 12-h HRRRv4 forecast valid 00z 13 March 2020.

iii. Relative humidity with respect to precipitable water

A total-column RH with respect to precipitable water (RHPW) is defined as the ratio between precipitable water (PW) and PW if the full column was completely saturated with respect to water, i.e., ***RHPW = PW / PW(sat)***. Figure 4 shows an example of RHPW. RHPW provides more continuity, especially across terrain variations, than PW (compare Fig. 4 below with Fig. 3 above). It is a relative-humidity measure through *all* levels, more so than the 850-500 hPa RH product (Fig. 2). RHPW shows similar patterns to 850-500 hPa RH. The 850-500 hPa RH gives a linear average of RH over pressure intervals. RHPW is weighted more heavily toward layers with warmer temperatures and much higher saturation vapor pressure; i.e., a 'Clausius-Clapeyron-weighted' measure of vertically integrated RH.

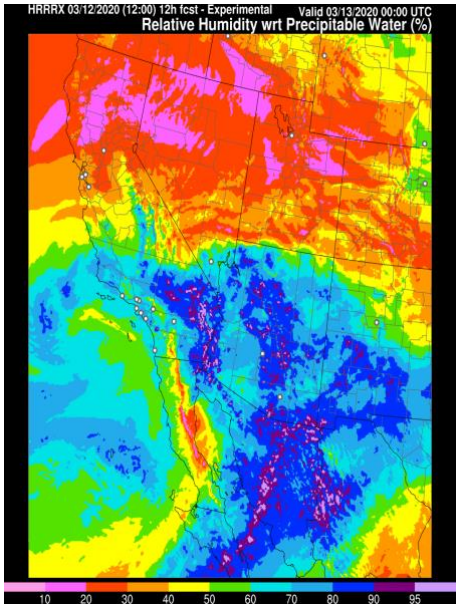

Fig. 4. Relative humidity with respect to precipitable water (RHPW). From 12-h HRRRv4 forecast valid at 00 UTC 13 Mar 2020, same forecast shown in Fig. 3.

B. Surface and boundary-layer variables

i. 2-m temperature

The 2-m temperature (Fig. 5) is diagnosed internally in the model in a surface-diagnostics subroutine in the forecast model using atmospheric temperature, skin temperature, and sensible heat flux at the surface. This field is diagnosed because the lowest model level in sigma coordinates is currently 0.999-sigma or ~8 m above ground level (AGL).

The 2-m temperature is valid at 2 m above the *model* terrain elevation at the same grid point. For comparisons with observations, users should apply a correction for the observation-minus-model elevation difference using the local lapse rate (as used in data assimilation for HRRR, RAP, and RRFS; Benjamin et al. 2016a, section 2.a).

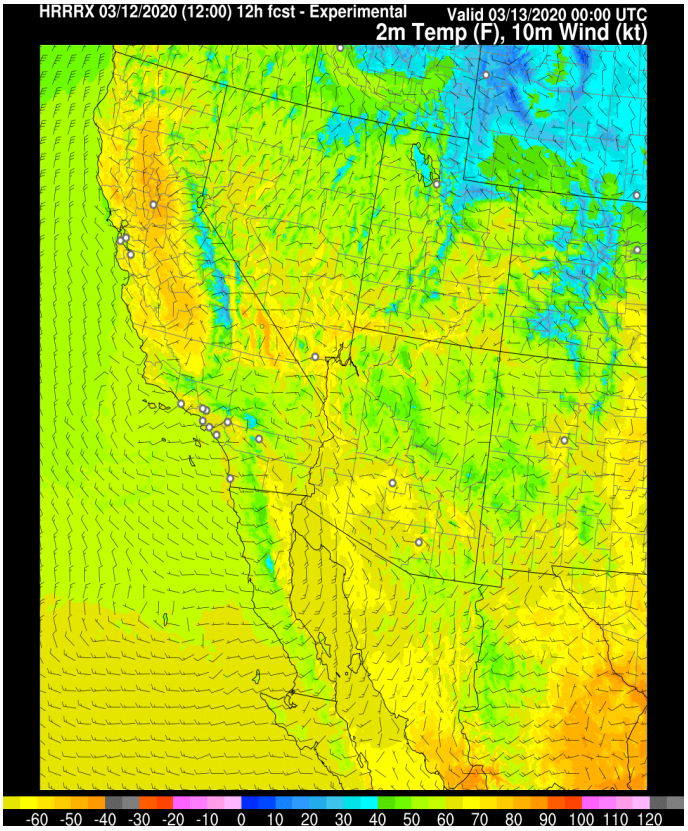

Fig. 5. 2-m temperature.

ii. 2-m dewpoint

The 2-m dewpoint temperature (Fig. 7) is calculated directly from temperature, specific humidity, pressure and surface latent heat flux. HRRR, RAP and RUC models used a flux-formulation diagnosis of the 2-m specific humidity value (Benjamin et al. 2016a, section 2.f) using the surface latent heat (moisture) flux under unstable conditions (Fig. 6). RRFSv1.0 uses a linear-interpolation diagnosis between the surface and lowest model level, resulting in a higher estimate of 2-m specific humidity (and subsequent calculation of 2-m dewpoint). As of this writing, RRFSv1.1 and RRFSv2 are planned to revert to the flux-formulation diagnostic of 2-m specific humidity. The flux 2-m diagnostic is considered to be more accurate while the linear 2-m diagnostic exaggerates 2-m dewpoint estimates in daytime leading to an erroneous drying effect in data assimilation in RRFSv1.0.

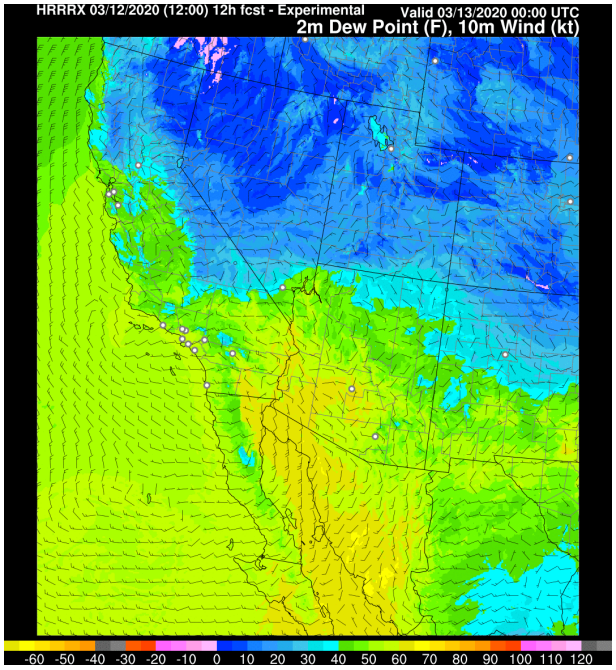

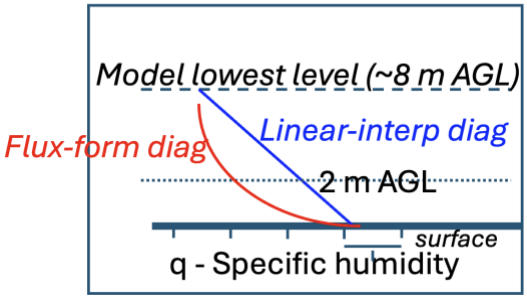

Fig. 6. Methods for diagnosis of 2-m specific humidity. The flux-based estimate (red) gives an exponential variation between the surface and the lowest model level (~8 m above ground level - AGL). The linear-interpolation method (blue) gives a linear variation. The horizontal axis is for magnitude of specific humidity; vertical axis is height above ground.

Fig. 7. 2-m dewpoint temperature. 2-m dewpoint (displayed in ºF) combined with a wind barb display of 10-m wind (in knots, long barb = 10 knots, half barb = 5 knots). Shown here are 12-h forecasts valid 00z/13 Mar 2020 from the 12z/12 Mar 2020 HRRRv4.

iii. 10-m wind (instantaneous and maximum)

The 10-m wind is calculated directly by interpolation accounting for stability between the lowest two model levels within the forecast model. The lowest prognostic model level in HRRR, RAP and RRFS is about 8 m AGL at sea-level, slightly less for higher elevations.

An hourly maximum 10-m wind speed is also diagnosed from values at each model time step for each horizontal grid point.

iv. 80-m wind speed (plus additional lower-tropospheric levels)

The 80-m AGL wind speed is estimated internally within the forecast model by interpolation between the appropriate prognostic model levels. Wind speed at this level has been useful as a nominal hub-height wind speed for wind energy applications, but it is also useful as another metric for wind gust potential. Additional levels (30, 50, 100, 160, and 320 m AGL) were included with RRFSv1 to account for higher wind turbines and provide more data points in the lowest 50 m for maritime search-and-rescue operations .

v. PBL depth

The PBL height (above ground level) is diagnosed directly in the model MYNN PBL scheme (Olson et al. 2019a,b) using a hybrid PBL diagnostic based on turbulent kinetic energy when the sensible heat flux is low (stable conditions) and based on the virtual potential temperature (θ_v) profile when sensible heat flux is positive. The θ_v profile uses the model native levels and the lowest-level θ_v value is boosted by an additional 0.5 K, which does not strongly affect the PBL height if it is already at least 100 m, but does avoid a diagnosis of zero depth from a small (< 0.5 K) inversion in the lowest 20 m.

An example of a PBL height field is shown in Fig. 8. **Note**: A separate PBL depth using only the θ_v profile continues to be used for diagnosing *potential wind gust speed as shown in Fig. 9*.

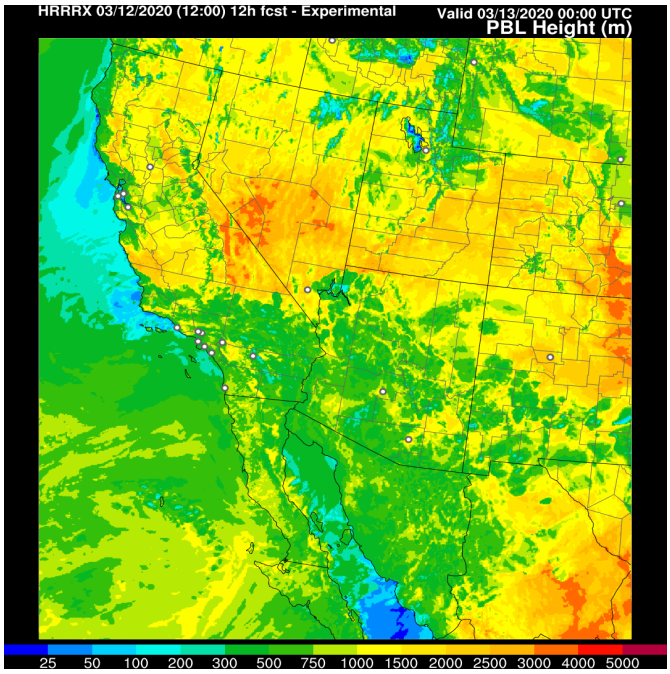

***Fig. 8. Planetary boundary layer (PBL) height (m).* Above ground level.** From the 12-h HRRRv4 forecast valid at 00 UTC 13 Mar 2020.

vi. Potential wind gust speed

The *potential* wind gust speed diagnostic depends on the PBL depth diagnostic (above). It will often exceed the observations of transient wind gusts at a particular time and will generally exceed a simpler 1.6 x 10-m-wind-speed estimate but provides a better estimate of the higher-end maximum gusts possible. The diagnostic (see Fig. 9) calculates the excess of wind speed over the 10-m wind speed at each level below the PBL depth. This excess is then multiplied by a coefficient **(f(z))** that decreases with height from 1.0 at the surface to 0.5 at 1 km height AGL, and is 0.5 for any height > 1 km AGL. The maximum weighted wind excess is then added back to the surface wind [i.e., **gust-potential = vsfc + max (f(z)*(v(z)-vsfc))** where v(z) is the wind speed at some level *z* meters AGL and vsfc is wind speed at lowest model level]. This calculation is roughly illustrated by the graphic below (Fig. 9).

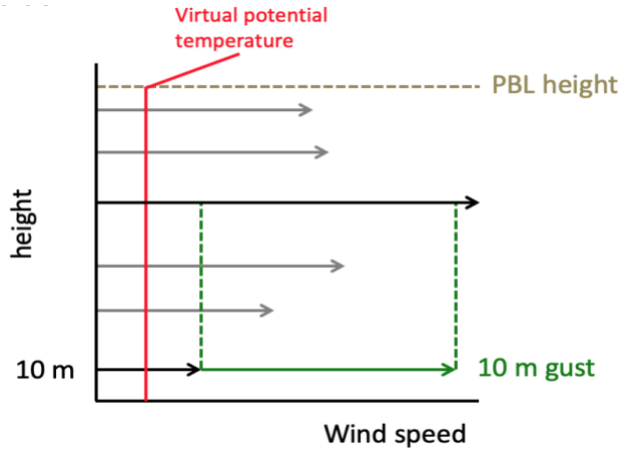

Fig. 9. PBL height and potential wind gust speed diagnostic. The horizontal axis is for both wind speed and for virtual potential temperature (in red).

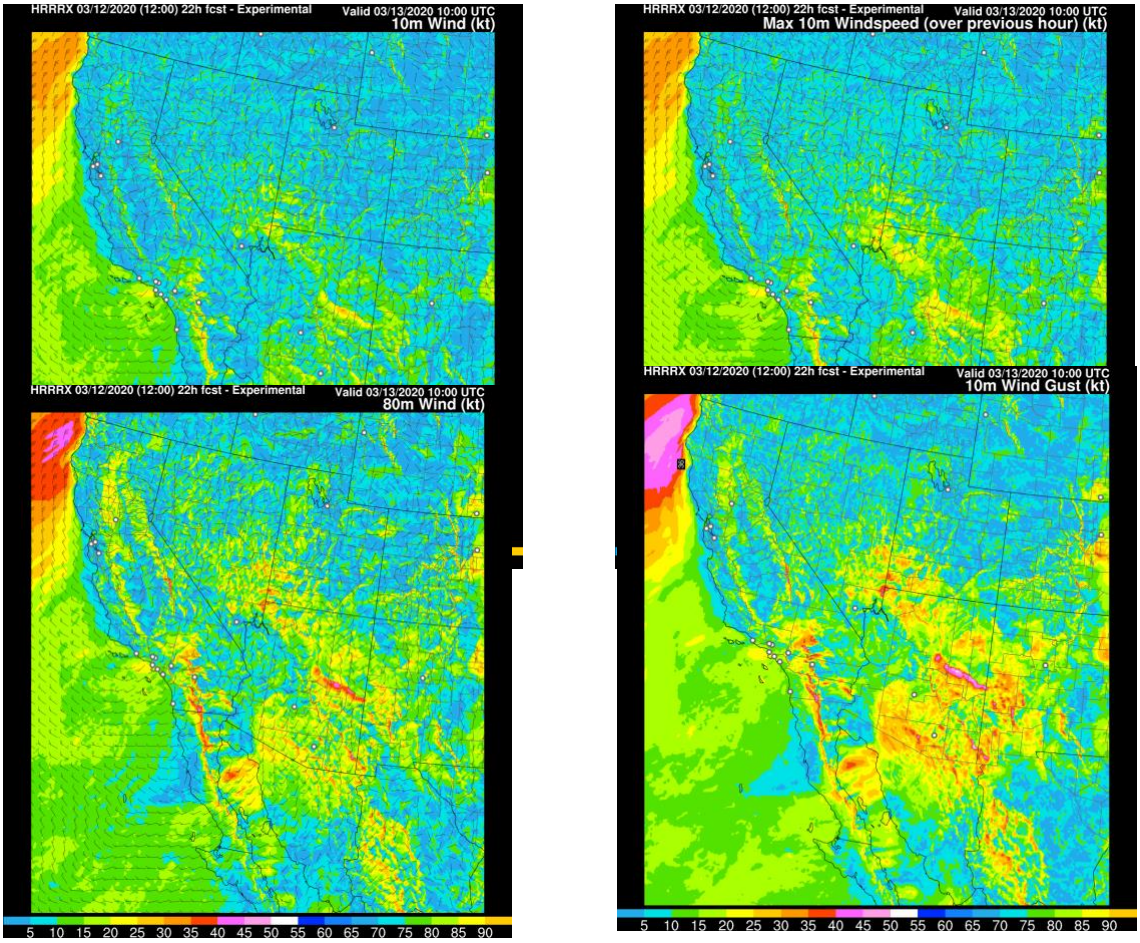

Fig. 10. Near-surface wind fields for 22-h HRRRv4 forecasts (kts) valid at 10 UTC 13 Mar 2020. This is the approximate time of the strongest wind downstream of the Mogollon Rim in Arizona following passage of an upper-level trough axis. Panels show (top left) 10-m winds, (top right) maximum 10-m wind over previous hour, (bottom left) 80-m winds, and (bottom right) **10-m potential wind gust speed.** There are instances when the 80-m wind may give the best forecast of the maximum 10-m wind gust potential.

C. Surface-pressure-related variables

i. Surface pressure

The hourly updated NOAA weather prediction models (HRRR, RAP, RRFSv1) all output surface pressure fields, the prognostic pressure at the atmospheric surface defined by the model terrain elevation field. The surface pressure is shown in Fig. 11 at the same time for the HRRRv4 and RRFSv1 models. Those two models have slightly different terrain elevation fields and their horizontal grids are defined differently, and the surface pressure fields are similar.

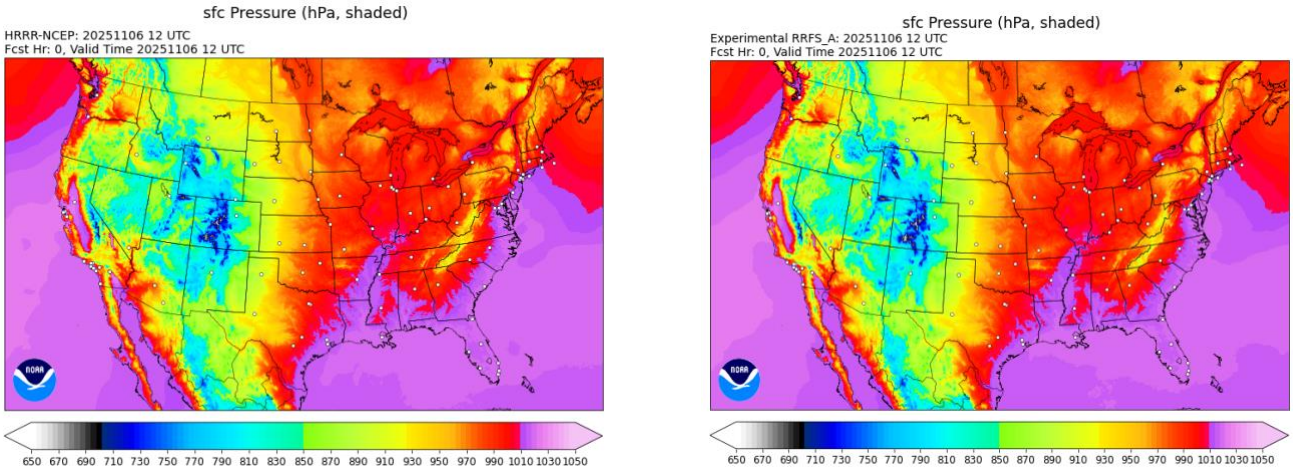

Fig. 11. Surface pressure. For 0-h (analysis) valid at 12 UTC 6 November 2025 for HRRRv4 (left – MAPS reduction) and RRFSv1 (right – MSLET reduction) models.

ii. Sea-level pressure

Two different sea-level pressure (SLP) reductions are used in the different hourly updated prediction models.

The RAP and HRRR use the MAPS reduction (Benjamin and Miller 1990) to calculate sea-level pressure. This reduction uses the 700-hPa temperature to minimize unrepresentative local variations caused by local surface temperature variations (used in most other reduction methods). This method improves over the standard reduction method in mountainous areas and gives geostrophic winds that are more consistent with observed surface winds (Fig. 11). The MAPS SLP includes some horizontal smoothing before output.

In contrast, RRFSv1 outputs the NAM (or 'Mesinger') SLP reduction (Pauley 1998, Mesinger and Treadon 1995), also called 'MSLET' since this mean-sea-level reduction was developed originally for the NOAA Eta regional model and later used for the NOAA NAM regional model. MSLET uses unsmoothed atmospheric fields and computes below ground extrapolated temperature by relaxing Laplace's equation. Differences in the output field smoothing contribute to the different appearance in Fig. 12 (MAPS SLP is smoothed, MSLET is not), but MSLET is intrinsically smoother than the MAPS SLP reduction.

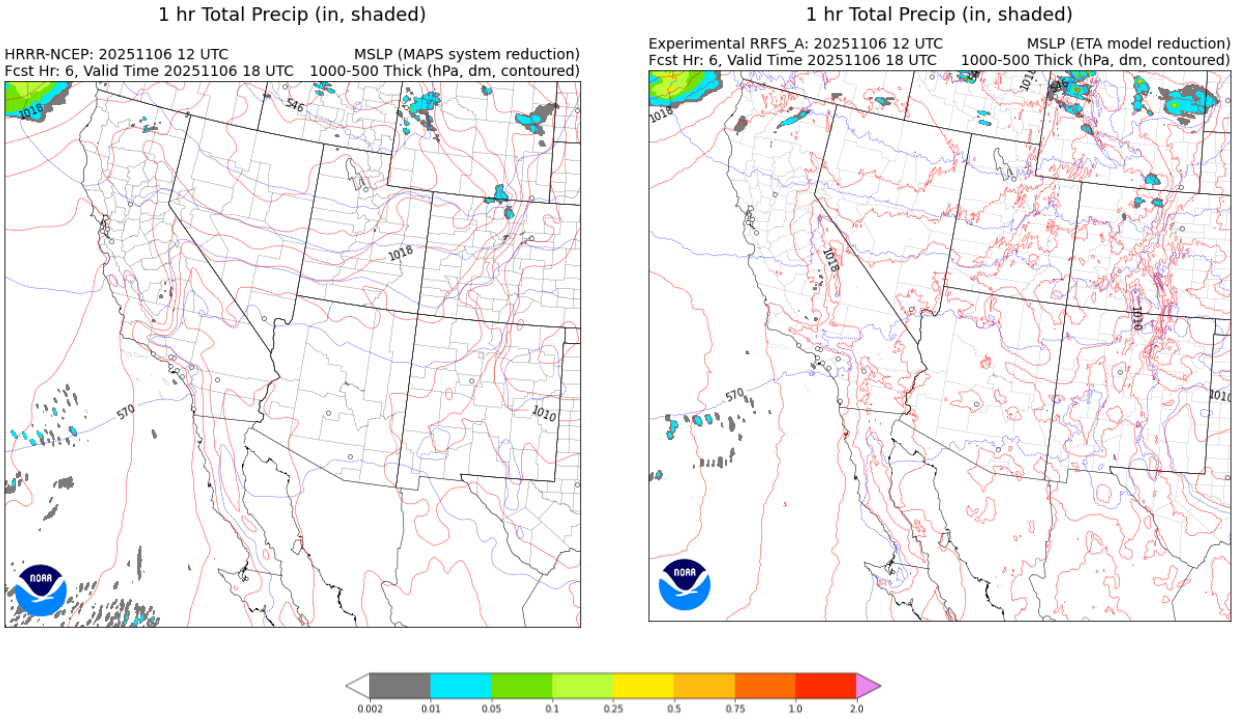

Fig. 12. Sea-level pressure. SLP is displayed for both HRRRv4 (left) and RRFSv1 (right) at the same time with their different SLP reduction techniques (see text). SLP is red-contoured (every 2 hPa) with the 1-h total precipitation field as a graphic (in inches). 1000-500 hPa thickness is also shown (dm, blue). Shown here are 6-h forecasts valid 18 UTC 6 November 2025 from the 12 UTC model forecasts.

D. Soil-land-lake-related variables

i. Soil temperature and moisture

Soil moisture at different levels is cycled continuously in the RAP/HRRR model/assimilation cycles without resetting from external models. There are 9 levels in the RUC land-surface model (RUC LSM -Smirnova et al 2016, Smirnova and Benjamin 2025 - SB25) used in the RAP, HRRR, and RRFSv1 models, with 4 levels in the top 10 cm and extending down to 3 m deep. Soil moisture fraction is calculated as the soil volumetric moisture divided by the full volume of the soil. The *surface* soil moisture (fraction) is for the top 0.5 cm of soil only, so this field responds quickly to recent precipitation or surface drying. In general, as soil depth increases, soil conditions change more slowly. The maximum soil moisture fraction is dependent on the soil-type-dependent value of porosity. Fig. 13 shows soil moisture fraction at the surface, and at 30-cm depth, while Fig. 14 shows soil moisture availability (soil moisture at top level divided by maximum soil moisture at field capacity, Smirnova et al 1997). Soil temperature (Fig. 13) is defined at the same 9 levels in the RUC LSM.

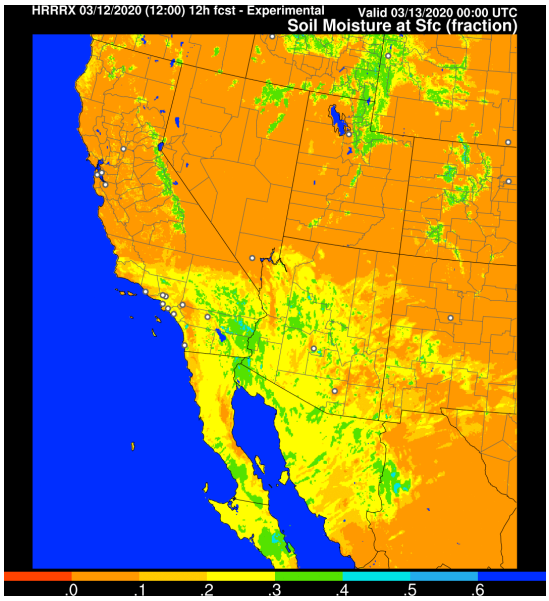

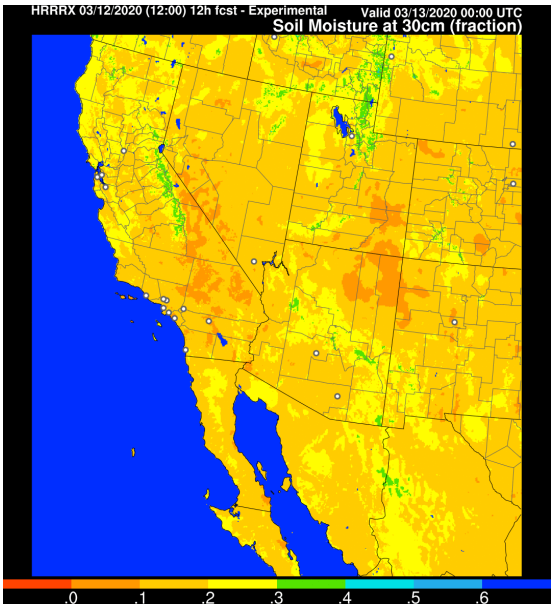

Fig. 13. Soil moisture fraction. 12-h HRRRv4 forecasts from the 12z/12 Mar 2020 run valid at 00z/13 Mar for two of the 9 levels of moisture in the land-surface model, the surface (0.5 cm) on the left and for a depth of 30 cm on the right. This variable is the fraction of soil moisture at a given level over the total possible moisture with field capacity (Smirnova et al 1997).

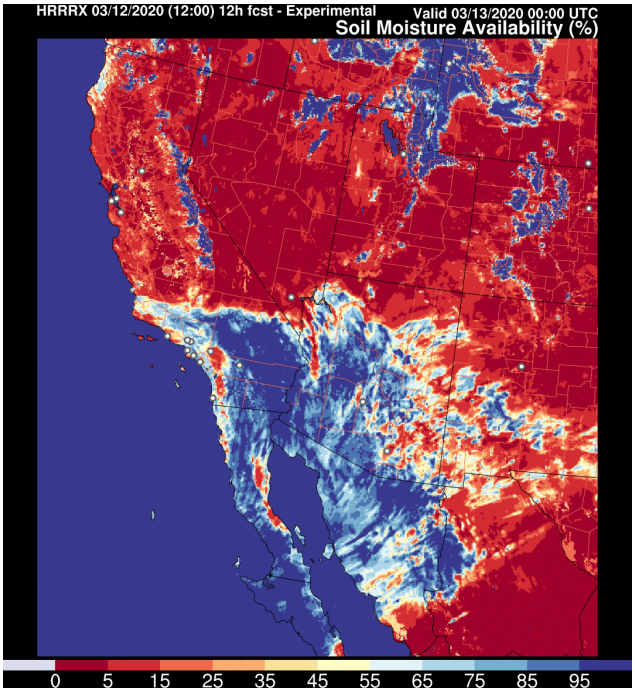

Fig. 14. Soil moisture availability. Units - percent, calculated in the top 0.5 cm layer. This is again a 12-h forecast valid 00z/13 Mar 2020 from the 12z/12 Mar HRRRv4.

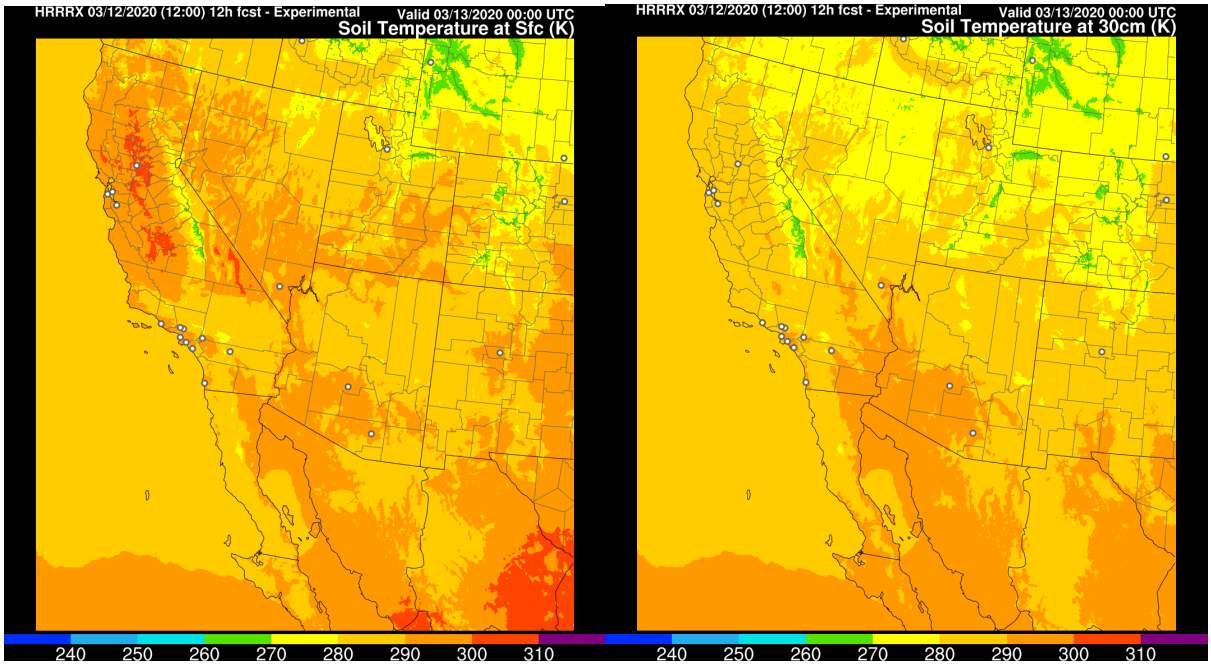

Fig. 15. Soil temperature (K) for surface (top 0.5 cm -left) and 30-cm level (right). From 12-h HRRRv4 forecasts from the 12z/12 Mar 2020 run valid at 00z/13 Mar.

ii. Skin temperature

Skin temperature (Fig. 16) is the temperature of the top level (1-cm depth) in the 9-level soil model (Smirnova et al 2016) over land, and the sea-surface (or lake-surface) temperature over water. Skin temperature will also be from the top snow level (up to 7.5 cm deep, Smirnova et al. 2000) in the 2-layer snow model for grid points with snow cover. Skin temperature will vary in time for soil and snow-covered grid points, and starting with HRRRv4 and continuing with RRFSv1, also for small lakes (Benjamin et al. 2022b, Trahan et al 2025).

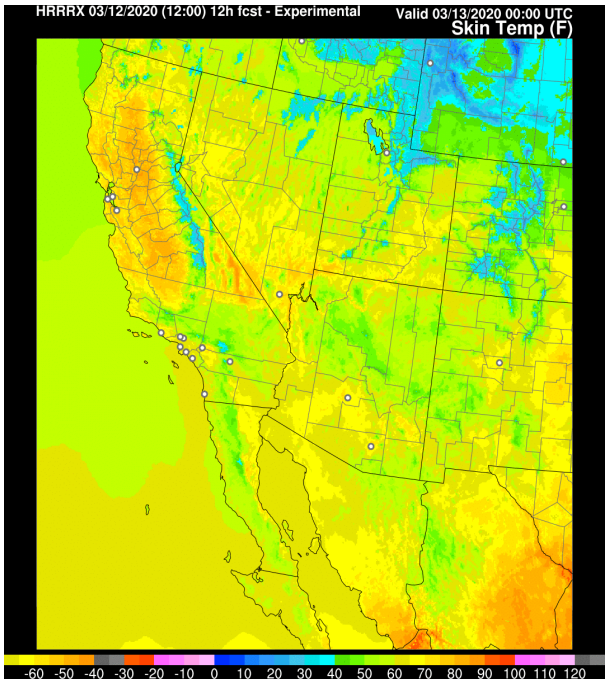

Fig. 16. Skin temperature. From 12-h forecast valid 00z/13 Mar 2020 from the 12z/12 Mar HRRRv4. Graphic in ºF.

E. Precipitation variables

i. Precipitation

All precipitation values in the RAP, HRRR and RRFSv1, for all accumulation intervals including the model run total, are *liquid equivalents*, regardless of whether the precipitation is rain, snow, or other frozen precipitation. (In one exception, snow accumulation products are available both for liquid equivalent and in snow depth using temperature-dependent variable density instead of a simple 10:1 snow/water ratio). The run-total accumulated precipitation is the precipitation accumulated since the model initialization time. The 1-h precipitation is the precipitation accumulated over the previous hour. The 15-minute precipitation (available in HRRRv4 and RRFSv1) is the precipitation accumulated over the previous 15 minutes. Note that the RAP and HRRR do not output 3-h or 6-h precipitation, although these can be calculated by differencing the appropriate output files. The instantaneous precipitation rate is the total precipitation (resolved and sub-grid-scale) from the last physics time step and is written in mm/s.

In contrast to HRRR, RRFSv1 uses a convective parameterization at its similar 3-km resolution as shown in Table 2. At 13-km resolution, the RAP also uses a convective parameterization scheme to represent sub-grid precipitation using the Grell-Freitas (2014) scheme .

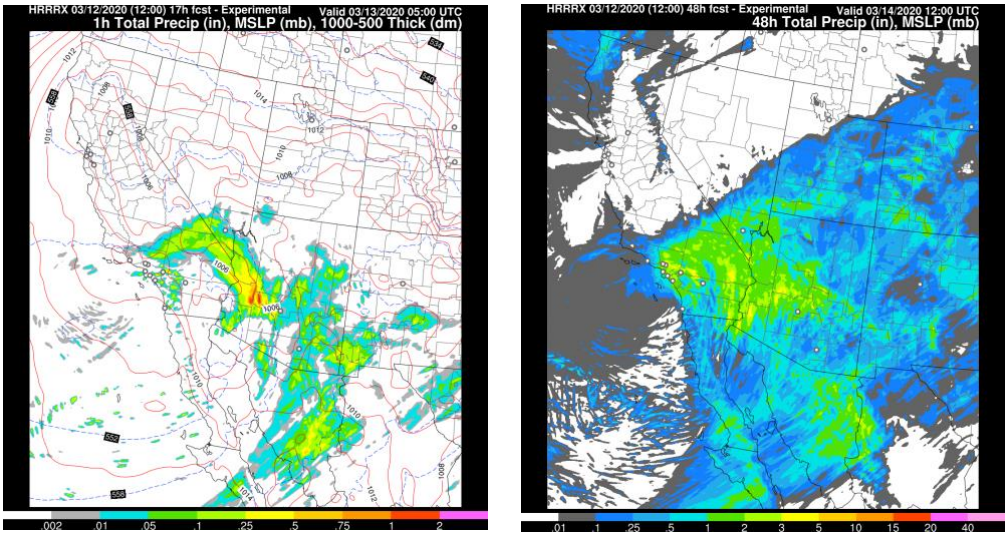

The various precipitation fields available on the HRRR/RAP websites are shown below (Figs. 17-25).

Fig. 17. Basic precipitation fields: *1-h precipitation and MSLP (left) and run-total precipitation (right), in inches for HRRRv4 forecast initialized 12 UTC 12 Mar 2020.*

ii. Snow/sleet accumulation

Two products are available for snow accumulation using **fixed** or **variable density**.
This **fixed-density snow accumulation** is calculated using a **10:1 snow-water ratio (SLR)** from the snow mixing ratio (using Thompson cloud microphysics) reaching the surface over the accumulation period. SLR varies in reality, but the ratio used for this product was set at this constant value so that water content is unambiguous. The snow accumulation (through the snow liquid water equivalent) is explicitly forecast through the mixed-phase cloud microphysics in the model and specifically from snow mixing ratio fall out to the surface. Therefore, both fixed (10:1 SLR) and variable snow accumulation are based on only snow fallout at the surface and do not include graupel fallout.

The Thompson (Thompson et al. 2008, Thompson and Eidhammer 2014) microphysics used in RAP and HRRR calculates explicitly the fall of snow mixing ratio (*qs*), graupel mixing ratio (*qg*), and rain mixing ratio (*qr*) reaching the surface, using separate fall speeds for each. This allows separate diagnosis of accumulation for each variable.

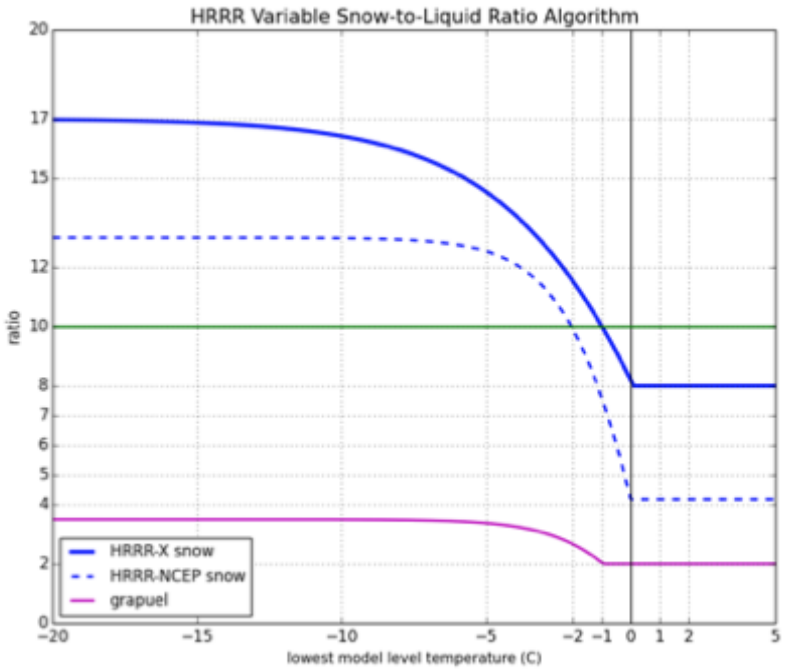

The ***variable density* snow accumulation** uses a crude near-surface-temperature-based estimate of snow-water ratio from less than 5:1 up to 17:1 (Fig. 18).

Note: A separate *snow density for falling snow diagnostic* has been added for RRFSv1 as described in an upcoming section.

Fig. 18. Snow-liquid ratio (SLR, density) of run-accumulated snow as a function of near-surface air temperature each time step for **variable snow accumulation** product. The 'HRRRX' curve is used for both HRRRv4 and RRFSv1. 'HRRR-NCEP' is from previous versions of HRRR (v1-v3) and RAP (v1-v4).

iii. Graupel accumulation

Graupel accumulation (Fig. 19) is defined as the model-internal accumulation at the surface, timestep-by-timestep, of graupel (*qg*) as defined by Thompson (2008) and Thompson and Eidhammer (2014). This graupel can occur from either winter-storm sleet or convective- storm ice/ graupel formation.

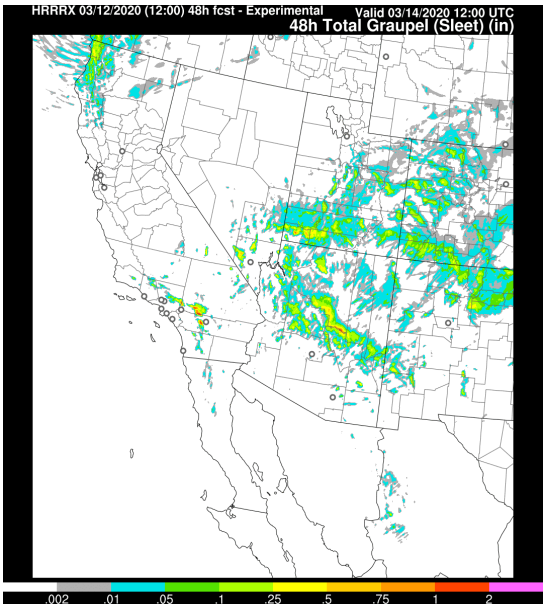

Fig. 19. Graupel accumulation. 48-h total accumulation of graupel ending at 12z/14 March from the 12z/12 March 2020 HRRRv4.

iv. Freezing rain accumulation

The freezing rain accumulation (Fig. 20) is calculated by accumulating a special class of rainfall, timestep-by-timestep, but only including values when the temperature at the lowest level < 0 ºC at that specific timestep. This variable is available for the 3-km models, HRRRv4 and RRFSv1, both using the explicit Thompson microphysics.

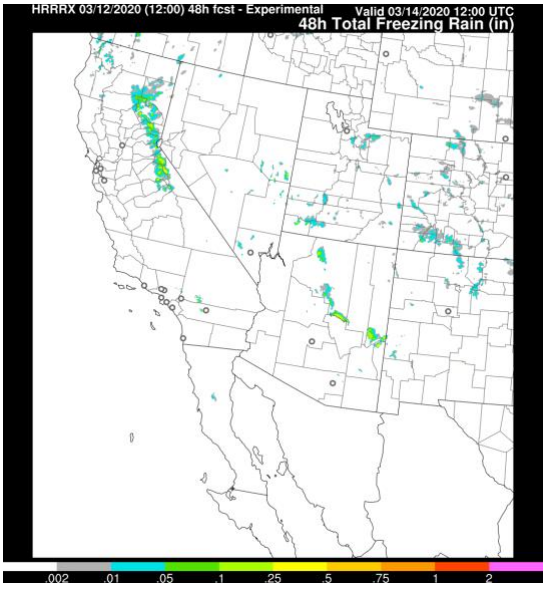

Fig. 20. Freezing rain accumulation. For 48-h total forecast accumulation ending at 12z/14 March from the 12z/12 March 2020 HRR

v. Frozen precipitation percentage

This field (Fig. 21) uses the explicit precipitation (rain, snow or graupel) produced from the multi-species Thompson cloud microphysics scheme. It is calculated as (snow-accumulated + graupel-accumulated) divided by (snow-accumulated + graupel-accumulated + rain-accumulated). No rime factor (as used on the Ferrier microphysics scheme - Aligo et al. 2018) is used in this explicit calculation.

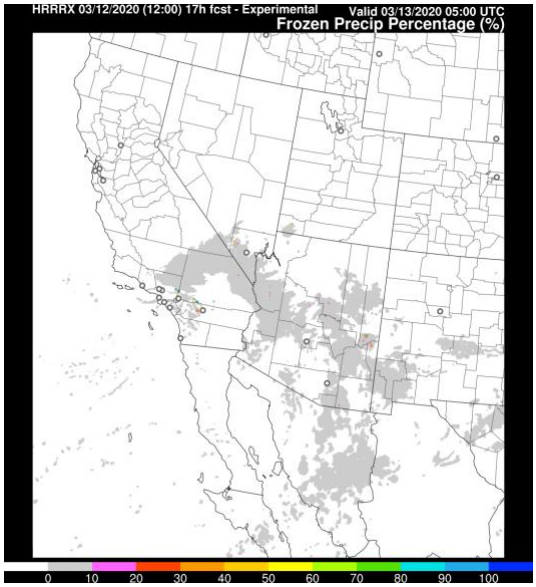

Fig. 21. Frozen precipitation percentage. For 17-h forecast valid for the previous 1-h period valid at 05z/13 March from the 12z/12 Mar 2020 HRRRv4.

vi. Snow depth

This field is the current estimated snow depth on the surface using the latest snow density, which is also an evolving variable (snow-water equivalent cycles internally within the RAP, HRRR or RRFS 1-h cycle). For the evolution of the snow height in the RUC land-surface model (RUC LSM), a 10:1 ratio is applied only for fresh snow falling on the ground surface when 2-m air temperature is below -15 ºC. When 2-m temperature is warmer than -15 ºC the density of falling snow is computed using an exponential dependency on 2-m temperature, and usually the ratio will be less than 10:1, but not less than 2.5:1. The density of snowpack is computed as the weighted average of old and fresh snow and changes with time due to compaction, temperature changes, melted water held within the snowpack, and addition of more fresh snow. (See Koren et al. (1999) for snow density formulations.) More information on snow depth evolution is described in Smirnova et al. (2016), Corrie et al. (2024, section 2.c) and SB25. This snow density is applied in the blowing snow diagnostic described later under the ‘visibility’ diagnostic.

HRRR/RAP and RRFS use the RUC LSM with a 2-level snow model and cold-season effects (freezing and thawing of moisture in soil, etc. - see Smirnova et al. 2016). These models all cycle snow depth/cover, respectively, as well as snow temperature in the top 5 cm and below that top snow layer. Fig. 22 shows snow-related variables from the HRRRv4.

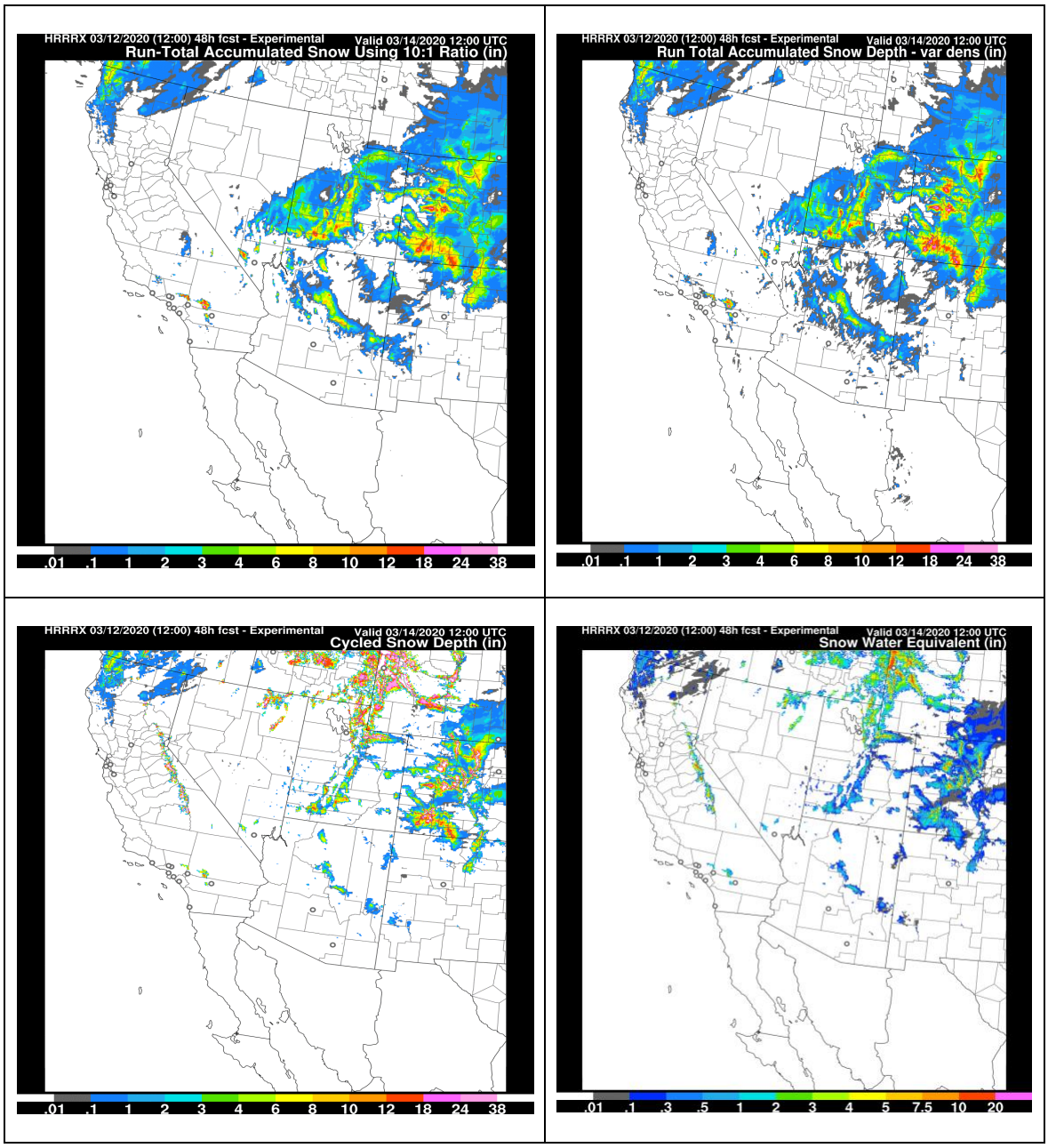

Fig. 22. Snow-related variables (all in inches) from HRRRv4 forecasts from the 12z/12 March run. **Accumulated snow applying a 10:1 ratio (upper left) and using variable density (upper right),** for the 48-h period ending 12z/14 March 2020. Also, 48-h forecast valid at 12z/14 March of **snow depth (lower left) and snow-water equivalent (lower right).**

vii. Snow-water equivalent. As described above, snow-water equivalent (SWE) is for all accumulated snow and graupel on the surface. SWE increases from accumulation and decreases from melting. SWE does not change from snow compression (which is represented in the RUC LSM). SWE processes in HRRR, RAP, and RRFSv1 are described in both Smirnova et al (2016) and SB25. The RRFSv1 application of the RUC LSM is described in more detail in SB25.

viii. Precipitation type(s) – potential area

Yes/no categorical indicators for rain, snow, ice pellets, and freezing rain potential are calculated from the 3-d hydrometeor mixing ratios reaching the ground in the explicit Thompson cloud microphysics parameterization in the HRRR, RAP and RRFS models. Details on the diagnosis of this explicit precipitation-type diagnosis were important and detailed enough to warrant a full journal article: Benjamin et al. (2016b). A decision tree for the diagnosis is provided in Fig. 23, and an example forecast is shown in Fig. 24.

The p-type (precipitation type) values from this explicit diagnosis are not mutually exclusive; more than one value can be yes (1) at a grid point, just as different hydrometeor species can coexist at a given 3-d grid volume in the Thompson cloud scheme. This non-exclusive diagnosis reflects what can occur in the real world also, e.g., mixed rain/snow, or mixed freezing rain and sleet. The accumulation thresholds used are very low, well below measurable thresholds, so the diagnostic will indicate **potential** areas of hazardous p-type conditions to increase the probability of detection and reduce unforecasted hazardous events. It should be combined with QPF and freezing rain accumulation and sleet accumulation values.

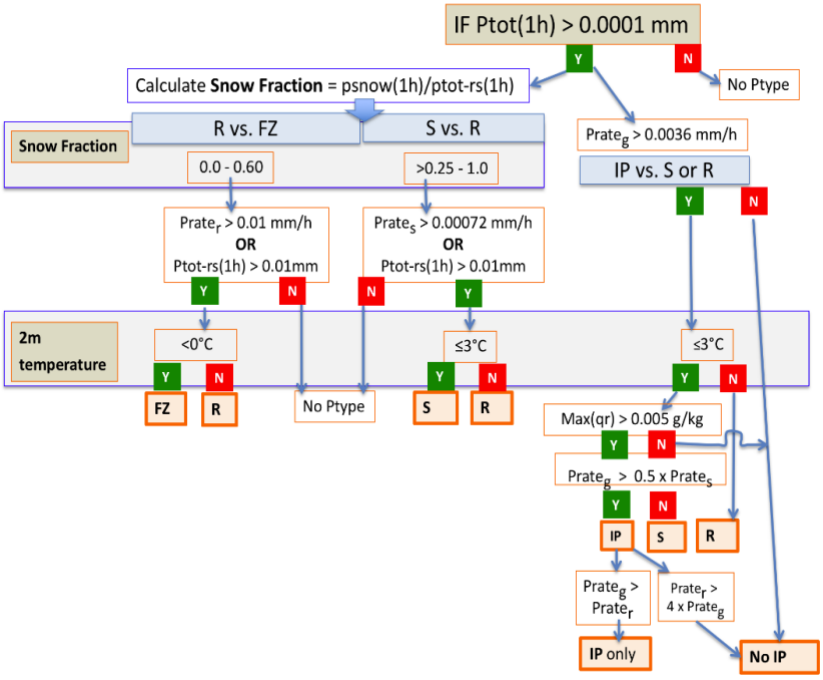

Fig. 23 - Explicit precipitation-type diagnostic method. From Benjamin et al. 2016b, Fig. 1. Flowchart describing the diagnostic logic for determination of precipitation type. (Bold letters in tan boxes: (**FZ, IP, R, S**) = (freezing rain, ice pellets, rain, snow). *Ptot*, *ptot-rs* and *psnow* are the total, rain plus snow (no graupel), and snow only (water-equivalent) precipitation, respectively, 1h indicating over the last hour. Prate is the instantaneous fall rate for different hydrometeor types (r – rain, s – snow, g – graupel). The maximum rain mixing ratio in the column is represented by Max(q_r).

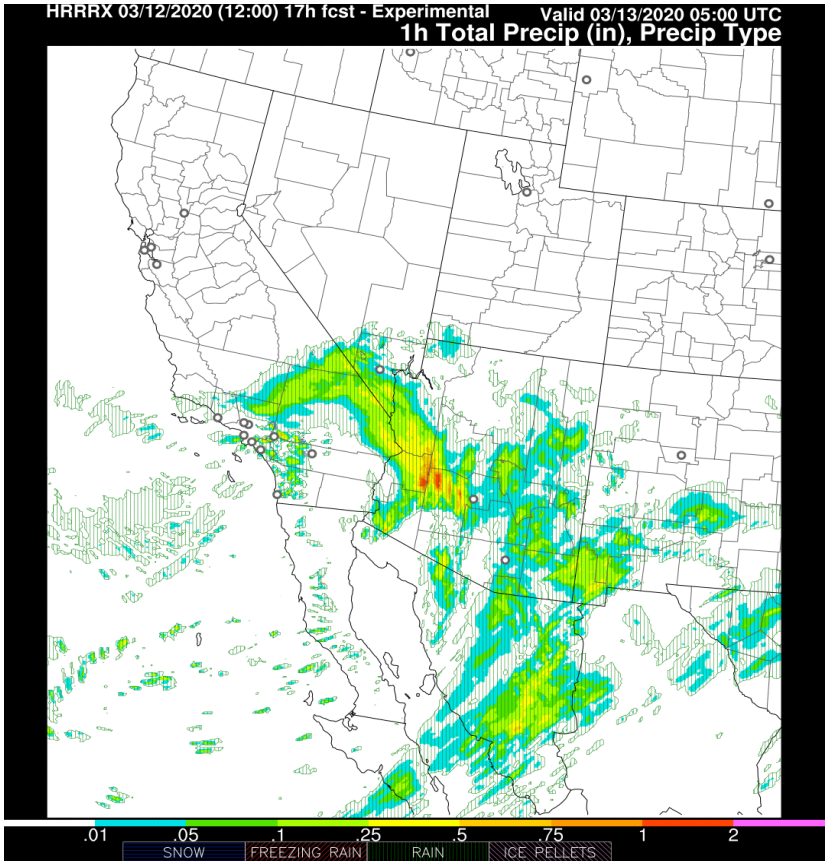

Fig. 24. Precipitation type. From 17-h HRRRX forecast valid at 05z/13 March combined with 1-h total precipitation (image) for the 1-h period ending at 05z/13 Mar.

ix. Maximum graupel/ hail size

The current HRRR output contains two diagnostics of maximum graupel/hail size (diameter) at the surface. The first diagnostic, which operates within the Thompson microphysics parameterization, calculates the maximum hail size directly from the calculated graupel size particle distribution. Beginning with HRRRv4, an additional hail diagnostic based on a one-dimensional hail growth model, referred to as HAILCAST (Adams-Selin and Ziegler 2016), is included in the HRRR output. RRFSv1.0 provides HAILCAST output only for maximum hail size, but future versions will likely include additional quantities. Output from the two hail-size diagnostics is shown in Fig. 25.

Hail-related diagnostic fields from versions of HRRR model:

HRRRv4	Hourly max vertically integrated graupel Thompson MP-based hourly and vertical column maximum hail size diagnostic Thompson MP-based hourly maximum surface hail size diagnostic HAILCAST hourly maximum surface hail size diagnostic

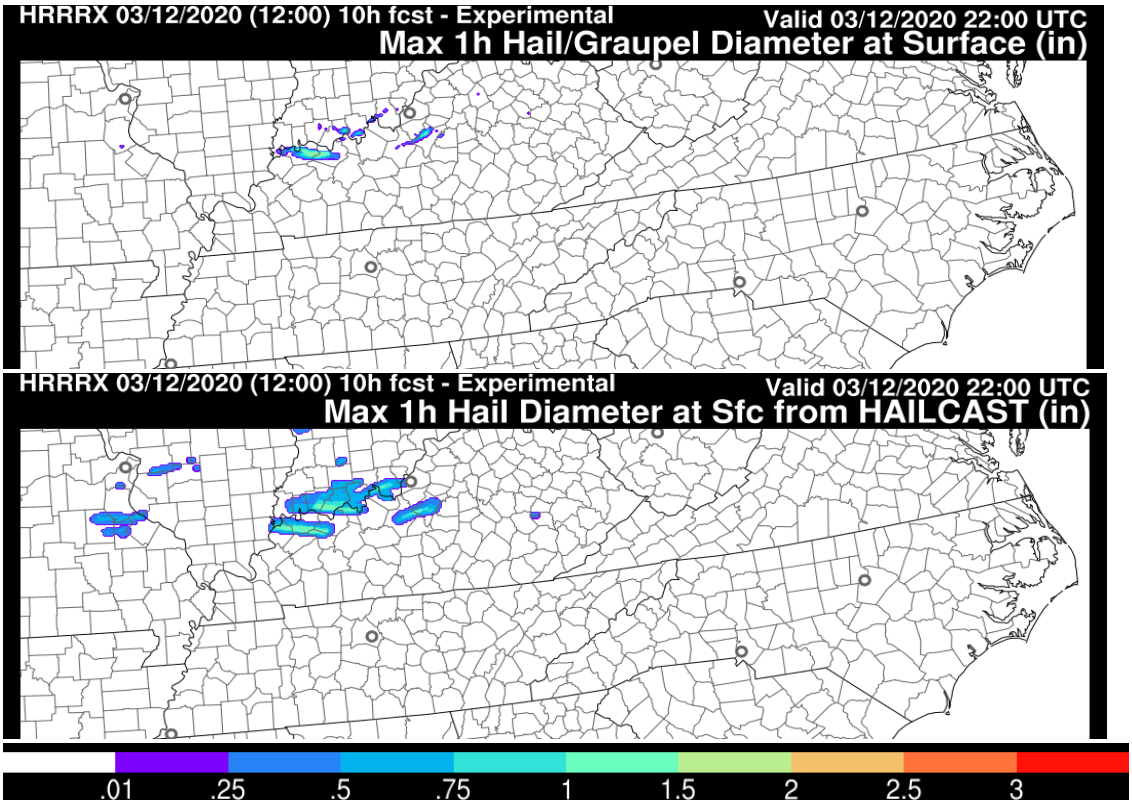

Fig. 25. Max hail/graupel diameter at the surface. 10-h HRRRv4 10-h forecasts from the 12z/12 March 2020 run valid at 22z/12 Mar at the surface for the 1-h ending at 05z (top), and maximum hail diameter using HAILCAST for the 1-h ending at 05z (bottom), both in inches, for a severe-weather event with accompanying supercell and other storms.

x. Precipitation rate.

This variable (units: m/s) is instantaneous in that it is calculated over the last time step (20 s for the HRRR, 60 s for the RAP, 36 s for RRFSv1). It is calculated solely from the explicit precipitation in the HRRR (i.e., via Thompson cloud microphysics) but in the RAP and RRFSv1, from combined explicit precipitation and parameterized precipitation.

xi. Snow density of falling snow

RRFSv1 provides an instantaneous snow-density field (GRIB2 variable: "SDEN") *of falling snow* that is obtained from the linear-regression algorithm of Pletcher et al. (2026), sometimes referred to as the *University of Utah SLR* (snow–liquid ratio) *algorithm*. This algorithm is intended to diagnose the instantaneous density of snow if snow were to be falling at a given location and time. Note that other snow-related fields in RRFSv1 (e.g., snow accumulation) are not currently formulated using the results of this algorithm. This falling-snow density is a different diagnostic from the temperature-dependent SLR technique shown above and in Fig. 18.

F. Severe-weather index variables

i. CAPE/ CIN/ EL (equilibrium level)

Convective available potential energy (CAPE) is defined in RAP, HRRR and RRFS using the standard Unipost (UPP) definition of CAPE including use of virtual temperature. CAPE values are provided for surface-based CAPE (based on lowest model level), most unstable CAPE (MUCAPE) in lowest 300 hPa, and mixed-layer (lowest ~50 hPa mixed) CAPE (MLCAPE), lowest 90 hPa and others (see GRIB inventory). The calculation of CAPE considers only positively buoyant contributions of the ascending air parcel, starting at the parcel's Lifted Condensation Level (LCL) and ending at the Equilibrium Level (EL).

Convective inhibition (CIN) indicates the accumulated negative buoyancy contributions for the ascending parcel, starting at the parcel's LCL and ending at its EL. By this definition, CIN is mainly accumulated between the LCL and the Level of Free Convection (LFC) and represents the negative buoyant energy that must be overcome in order for the parcel to become positively buoyant once it reaches its LCL. This is also the standard Unipost definition.

Equilibrium level (EL) indicates the highest positively buoyant level. This is also the standard Unipost definition. The EL provided is associated with the most unstable CAPE parcel (MUCAPE; using the parcel with highest θ_e in the lowest 300 hPa).

Examples of the different CAPE and CIN variables are shown below (Figs. 26-27) for the southeast map domain from the HRRR website for a case of severe convection using forecasts from the 12z/12 March 2020 HRRRv4 run.

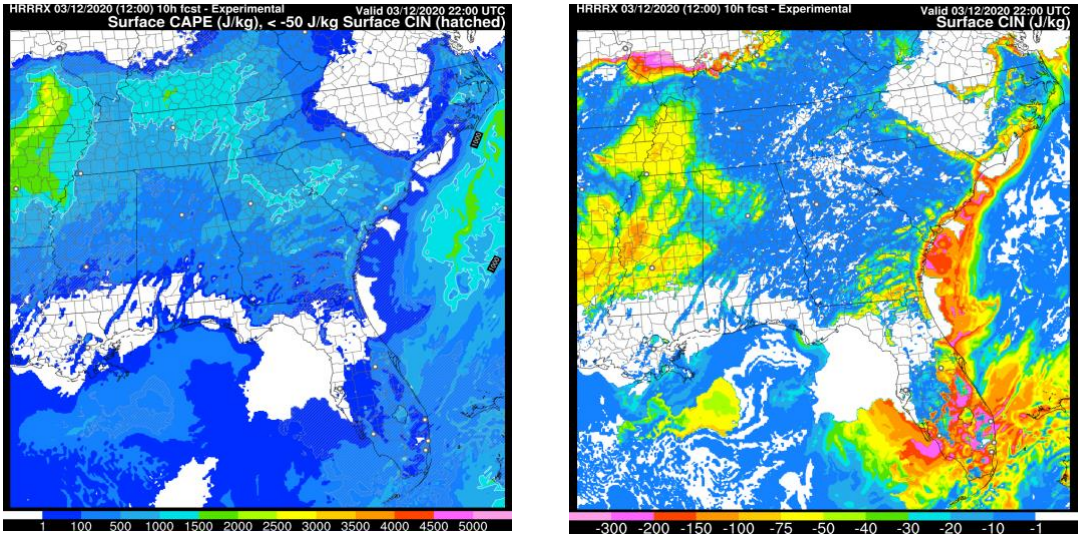

Fig. 26. CAPE/CIN variables. 10-h HRRRv4 10-h forecasts from the 12z/12 March 2020 run valid at 22z/12 Mar for (left) a combination of surface-based CAPE (image) with surface-based CIN (faint diagonal hatching for values less than -50 J/kg) and (right) for CIN only.

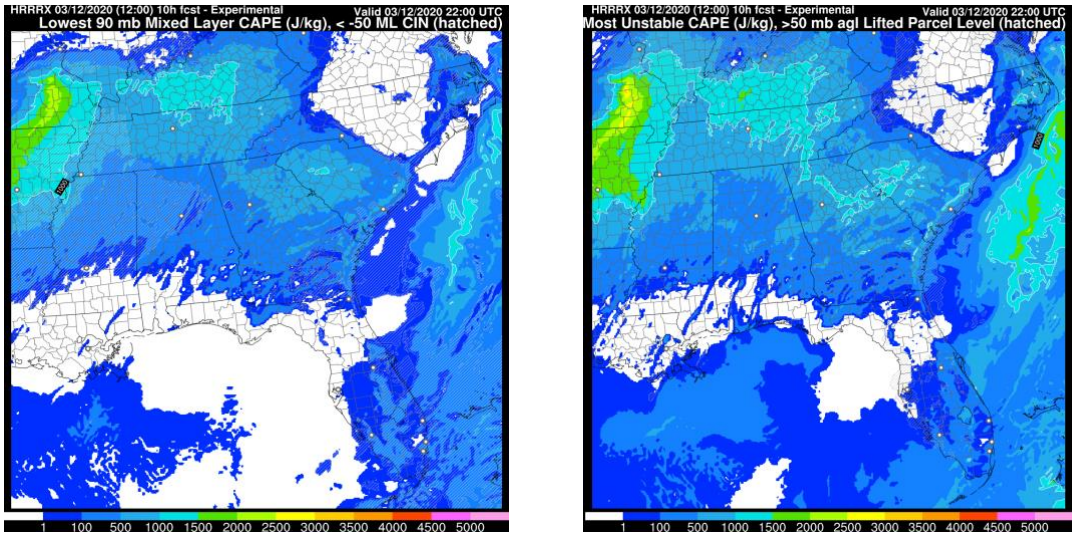

Fig. 27. Other CAPE and CIN variables. Top left figure shows an image for the **mixed-layer CAPE** with the mixed layer from the lowest 90 hPa, along with hatching where CIN (defined negative) has values below -50 J/kg. Top-right figure has an image for the **most-unstable CAPE** at any point in the atmosphere below the 300-hPa level with hatching if that point is above the lowest 50 hPa of the atmosphere (this distinguishes elevated instability from lower level or surface-based CAPE). Both figures show 10-h forecasts from the 12z/12 Mar HRRRv4.

ii. Lifted index (LI)

The lifted index (Fig. 28) indicates the difference between environmental temperature and ascending parcel temperature at 500 hPa (in K). The standard lifted index uses the surface parcel, and Best Lifted Index parcel uses the buoyant parcel from the native level with maximum buoyancy within 300 hPa of surface (also the standard Unipost definition).

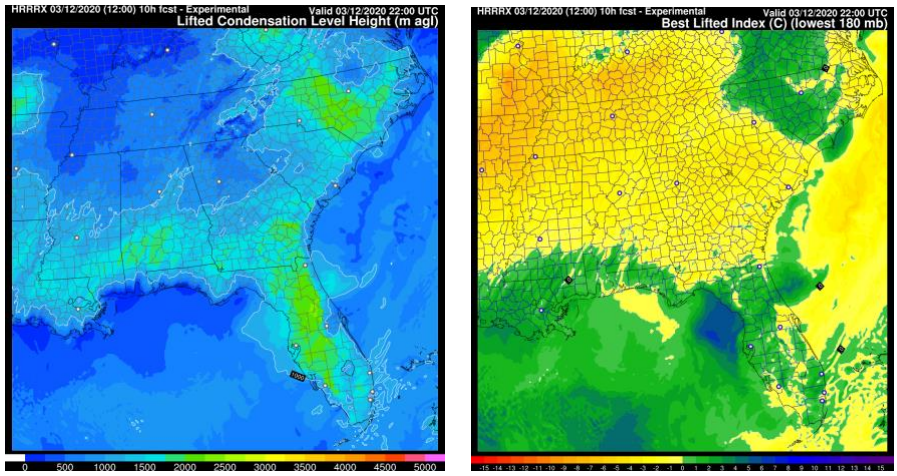

Fig. 28. LCL (left) and LI (right). 10-h HRRRv4 forecasts from the 12z/ 12 March 2020 run valid at 22z/12 Mar of Lifting Condensation Level (LCL, in m AGL, on left). LCL is calculated as the height at which the surface parcel becomes saturated with respect to liquid water when lifted dry adiabatically. Best Lifted Index (LI, ºC, using the best parcel in the lowest 300 hPa (caption incorrect) of the atmosphere) on right.

iii. Environmental helicity/storm motion

Environmental (not *storm-relative*) helicity and storm motion are defined following the diagnostics of Bunkers et al. (2000). Examples of vertical wind shear are shown in Fig. 29, and storm-relative helicity and storm motion in Fig. 30.

What can be considered high values of environmental helicity?
The units of helicity are $m^2\ s^{-2}$. The value of 150 $m^2\ s^{-2}$ is generally considered to be the low threshold for tornado formation. Helicity is closely related to low-level shear, so in high-shear situations, such as behind strong cold fronts or ahead of warm fronts, the values will be very large, possibly as high as 1500 $m^2\ s^{-2}$. High negative values are also possible in reverse shear situations.

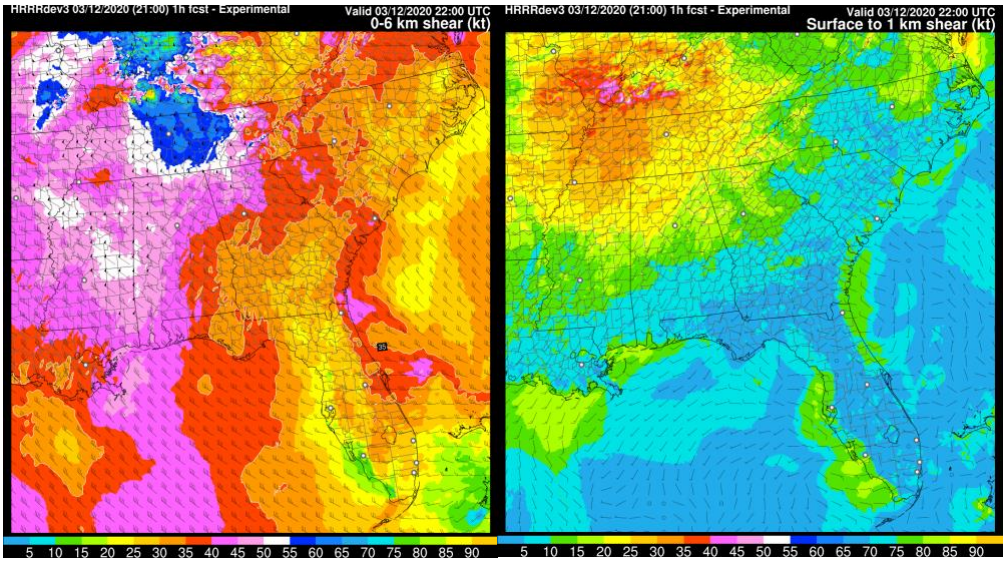

Fig. 29. 0-6 km (AGL) shear (left) and surface to 1 km AGL shear (right), both in knots. Shown are 1-h forecasts from HRRRv4 valid at 22z/12 March 2020.

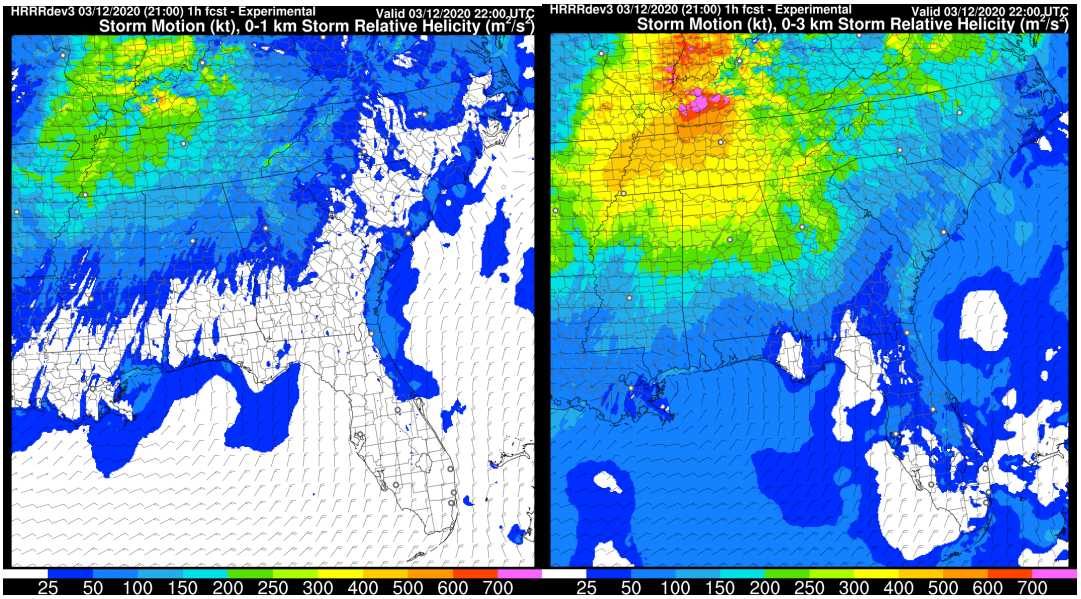

Fig. 30. Storm-relative helicity (SRH, in m^2/s^2) fields displayed with calculated storm motion. 0-1 km AGL SRH (left) and 0-3 km AGL SRH (right). Shown are 1-h forecasts from HRRRv4 valid at 22z/12 March 2020.

G. Cloud-related variables

In sections i-iii below, these descriptions apply to RRFSv1 only. We recommend looking at the previous tech memo (Benjamin et al. 2021a) for descriptions of the same cloud-related variables for HRRRv4 and RAPv5.

i. Cloud cover (i.e., cloud amount or cloud fraction) fields (various)

The MYNN PBL scheme (Olson et al. 2019a,b, 2026) provides a cloud fraction (0–1) in each grid volume and at each time step of the model integration. Using this instantaneous cloud-fraction field, numerous cloud-cover (percentage) fields are obtained, as described in Table 3.

GRIB2 variable*	Layer / Level	Description
TCDC:{hybrid level}	Single model layer	Cloud cover for each grid volume (3D field; no horizontal or temporal averaging)
TCDC:entire atmosphere	Column maximum	Maximum cloud cover for the applicable layer or column, as applicable (2D field; with horizontal averaging): (1) First, for each grid volume, a horizontal neighborhood average of cloud cover is obtained over a 16.1 km (10 mile) radius. This averaging serves as a horizontal smoothing operator. (2) Then, for the applicable layer/column, the maximum value of (1) is output.
LCDC:low cloud layer	Surface–642 hPa (~0–12 kft MSL)	
MCDC:middle cloud layer	642–350 hPa (~12–27 kft MSL)	
HCDC:high cloud layer	350–150 hPa (~27–45 kft MSL)	
TCDC:entire atmosphere (hourly average)	Column maximum	Hourly average of column-maximum cloud cover (2D field; no horizontal averaging)
TCDC:boundary layer	Surface–(PBL top+1 km)	Maximum cloud cover between the surface and the PBL top + 1 km (2D field; no horizontal averaging)

*Note that the GRIB2 field "TCDC" is formally described as "total cloud cover". Here, the sense of "total" is taken to include both explicit (resolved) and subgrid-scale (unresolved) clouds. Indeed, *all of the fields* in this table include both explicit and subgrid-scale clouds.

Table 3. Summary of cloud-cover fields available in RRFSv1.

ii. Cloud-base height and cloud-top height

In RRFSv1, the cloud-base height is the lowest level at which the cloud fraction is ≥ 0.02. In an analogous manner, the cloud-top height is the highest level at which the cloud fraction is ≥ 0.02.

iii. Ceiling height (two related fields)

The Federal Meteorological Handbook No. 1 (NOAA, 2019) defines ceiling as "the lowest layer aloft reported as broken or overcast; or the vertical visibility into an indefinite ceiling". In RRFSv1, two related ceiling fields are provided:

- The standard (main) ceiling field (GRIB2 variable: "**HGT:cloud ceiling**")

  Overview: The formulation of this diagnostic in UPP has been in longstanding use in the RUC, RAP/HRRR, and now RRFSv1 models. Because of its well-established history of operational use, it is sometimes referred to as the "legacy" ceiling diagnostic.

Description: Each model column is searched from the surface upward. A ceiling is diagnosed for any of three conditions:

1. ***When explicit (resolved) cloud hydrometeor masses exceed a threshold:*** Namely, the ceiling is assigned the lowest height for which the sum of resolved cloud-water (q_c) and cloud-ice (q_i) mixing ratios is ≥ 10^{-7} kg kg^{-1}. Note that a linear interpolation between model layers is performed, so this condition gives a continuous value.

    - Shallow-fog exclusion: When the threshold in (1) is exceeded at the lowest model layer—implying the existence of fog—an additional check is performed to assess the depth of the fog. Namely, if this threshold is also exceeded at level 2 (~32 m AGL) and/or level 3 (~80 m AGL), but not above that level, then the fog is characterized as too shallow to yield an aviation-affecting ceiling and is ignored.

2. ***When falling snow yields restrictive vertical visibility:*** When falling snow is present at the lowest model layer, a vertical visibility is calculated from the snow mixing ratio. This vertical-visibility calculation for snow uses the same formulation as ordinary (horizontal) visibility. If the vertical visibility is less than the ceiling height obtained by (1), then the vertical visibility is assigned as the ceiling.

3. ***When subgrid (unresolved) clouds are inferred:*** If the relative humidity at the PBL top is >95%, then the height of the PBL top is assigned as the ceiling. This condition is taken as an indication of unresolved (subgrid-scale) cloudiness. While crude, it nevertheless provides a key detection capability for this diagnostic.

- An alternative (supplemental) ceiling field (GRIB2 variable: "**CEIL:cloud ceiling**")

Overview: A secondary ceiling field is also available in RRFSv1, intended for aviation-oriented users who wish to consider ceiling guidance derived from an alternative diagnostic algorithm. GSL developers have found that this alternative ceiling field typically exhibits a reduced high-frequency bias (i.e., less excessive coverage) than the standard (or legacy) ceiling field, and this reduced bias may yield improved overall skill during the cold season. Interested users are generally advised to use this field *in conjunction with* the standard ceiling field, rather than discontinuing the use of the standard ceiling field.

Description: Each model column is searched from the surface upward. A ceiling is diagnosed for either of two conditions:

1. When cloud fraction exceeds a threshold: Namely, the ceiling is assigned the lowest height for which the cloud fraction is ≥ 0.41. A linear interpolation between model layers is performed, so this condition gives a continuous value. Note that the use of cloud fraction obviates the need to separately consider explicit (resolved) and

subgrid (unresolved) clouds. The threshold value of 0.41 was chosen based on experimental results.

- Shallow-fog exclusion: If a cloud fraction > 0 is present at the lowest model layer—implying the existence of fog—then the overlying model layers 2–4 are assessed to determine the depth of the fog. Namely, if cloud fraction is < 0.8 within any of these overlying layers, then the fog is ignored *at and below* these layers; i.e., the fog is too shallow to yield an aviation-affecting ceiling at these heights.

2. ***When falling snow yields restrictive vertical visibility:*** This condition is applied in an identical manner to that of the main ceiling diagnostic.

iv. Surface visibility

The surface visibility algorithm developed for and used in HRRR/RAP and RRFSv1 is an extension of the Stoelinga and Warner (1999) algorithm designed to take advantage of explicit hydrometeor types used in those models (Fig. 31 - RRFSv1). It is usable for any model with explicit hydrometeor predictions.

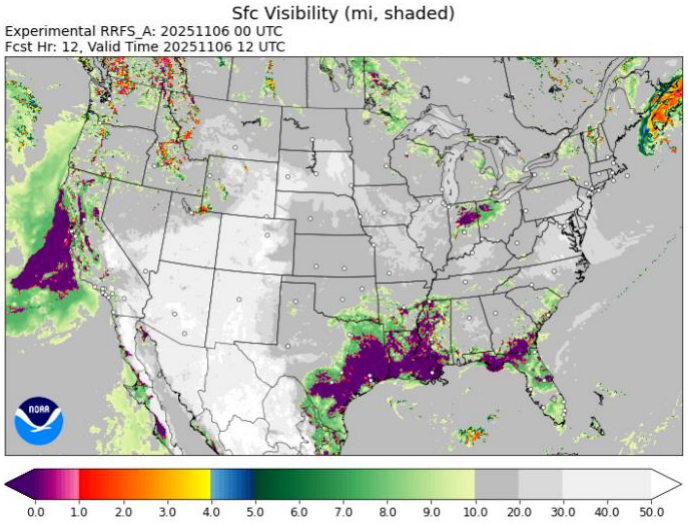

Fig. 31. Surface visibility (in miles). 12-h forecast from the 00z 6 November 2025 RRFSv1, valid at 12z 6 Nov 2025.

This visibility diagnostic is based on conditions at the lowest model level (about 8 m AGL) for these variables:

- Non-zero hydrometeors, with attenuation coefficients for each hydrometeor type (q_c, q_i, q_r, q_s, q_g). Maximum value of each hydrometeor type is calculated from the lowest 3 layers (from ~6-8m AGL up to ~60-75m AGL).
- day/night dependency for hydrometeor attenuation coefficients from Roy Rasmussen (NCAR, 2000)
- additional visibility attenuation term for forecast graupel hydrometeor mixing ratio
- additional relative humidity dependency (developed by GSL NWP team) using max RH at the lowest 2 levels. This RH term approximates the effects of haze on visibility. It allows a maximum 90-km (~56 mile) visibility with near-surface RH <15% and a minimum ~12-km (~7 mile) visibility with near-surface RH >95%.
- Smoke extinction (from 3-d smoke concentration at lowest level) is included beginning with RAPv5 and HRRRv4 (starting December 2020); dust extinction is included with RRFSv1 (see below).
- Blowing snow (see section G.v below, Corrie et al. 2024)

Generally, if hydrometeors are present at either of the two lowest levels (~6-8m and ~25-30m AGL), the diagnosed visibility will be less than 5-6 miles and usually, less than 3 miles. Otherwise (for estimated visibility > 7 miles), near-surface RH largely governs the visibility estimate. The inclusion of smoke effect is accomplished by assigning the overall surface visibility as the minimum of visibility from hydrometeors and smoke combined (each with their own extinction coefficients) vs. the visibility from RH.

v. Additional effect from blowing snow on surface visibility

An additional term (extinction coefficient) for blowing snow was added to the visibility diagnostic in the RRFSv1 model. This diagnostic is based on the time-varying snow density of snow on the ground and surface wind speed as described in Corrie et al. (2024). Snow density of snow on the ground evolves in time in the RUC land-surface model (RUC LSM) used in HRRR/RAP and in RRFSv1, which allows an estimate of the "driftability" of the snow cover.

vi. Additional effect of smoke and dust on surface visibility

Other additional extinction coefficients are added for smoke and dust. These extinction coefficients are calculated using both smoke aerosol concentration and dust aerosol concentration at the lowest model level.

vii. Shortwave and longwave radiative fluxes at surface and top-of-atmosphere

Instantaneous shortwave (SW) and longwave (LW) radiative flux fields are output from the hourly updated NOAA models. Downward SW radiative fluxes include total downward SW fluxes (units – W m^{-2}) and, separately, its direct and diffuse components. These fields are calculated using complex 1-d radiative transfer model parameterizations within the forecast models and are affected by all 3-d prognostic fields including cloud hydrometeor mixing ratios (cloud water, ice, rain, snow, graupel), predicted 3-d smoke concentration, and, for RRFSv1, predicted 3-d dust concentration. Note that the cloud hydrometeors used in the calculation of the radiation have both the resolved and subgrid-scale cloud components. Upward SW and LW fluxes at the surface (dependent on surface albedo, predicted soil and snow conditions, predicted surface emissivity, etc.) and top-of-atmosphere SW and LW fluxes are also output

viii. Simulated satellite imagery

HRRR and RRFSv1 have output synthetic simulated satellite imagery in the thermal infrared band (10.7 micron wavelength; Fig. 32a) and the water vapor band (6.5 micron wavelength; Fig. 32b), which is intended for comparison with GOES satellite observations. RRFSv1 has output for GOES bands 7-16. The simulated brightness temperatures are computed using the model output and the Community Radiative Transfer Model (CRTM; Han et al. 2006). The brightness temperature of clear grid points is calculated based on surface skin temperature, 10-m wind speed, pressure, and vertical profiles of temperature and water vapor. The brightness temperature of cloudy grid points uses vertical profiles of mixing ratio and number concentration for each hydrometeor species included in the Thompson-Eidhammer aerosol-aware microphysics scheme (Thompson and Eidhammer 2014). (Unfortunately, the simulated satellite

images do not include effects from subgrid-scale clouds (Olson et al 2019a, 2026).) Additional details about the formulation of the simulated brightness temperatures are provided by Griffin et al. (2017) and Otkin et al. (2007).

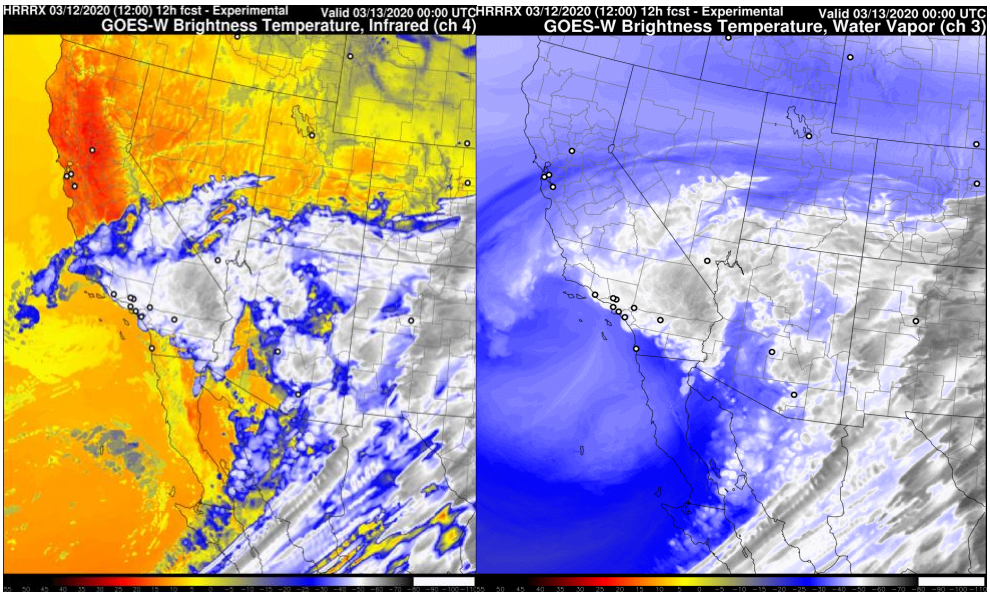

Fig. 32. Simulated IR and WV imagery. 12-h forecasts from the 12z/12 March 2020 HRRRv4 valid 00z/13 March for the simulated images from the GEOS-W perspective for IR channel 4 (left) and WV channel 3 (right).

H. Explicit-scale convective-storm variables

i. Radar reflectivity

Radar reflectivity products are produced in a different manner for hourly/15-min instantaneous and hourly maximum fields. For **instantaneous** fields with hourly or 15-min output, reflectivity is calculated using a **more sophisticated** method within the Thompson scheme for each model 3-d grid point based on rain, snow, graupel/hail, and temperature at that grid point. The temperature is used to determine if melting snow is present (i.e., if there should be a "bright band" in the computed reflectivity). The convective parameterizations used in RRFSv1 (see Table 2) and RAP also contribute to the diagnosed reflectivity.

These reflectivity diagnostics are produced:

- Composite reflectivity (maximum reflectivity in model column)
- 1-km AGL reflectivity (interpolated in model to 1-km AGL level)
- -10ºC reflectivity.

Hourly maximum fields using timestep-by-timestep calculations are produced for 1-km AGL and -10ºC reflectivity diagnostics. For these hourly maximum values, a **simpler** reflectivity diagnostic, not internal to the Thompson scheme, is applied. Examples are shown in Fig. 33.

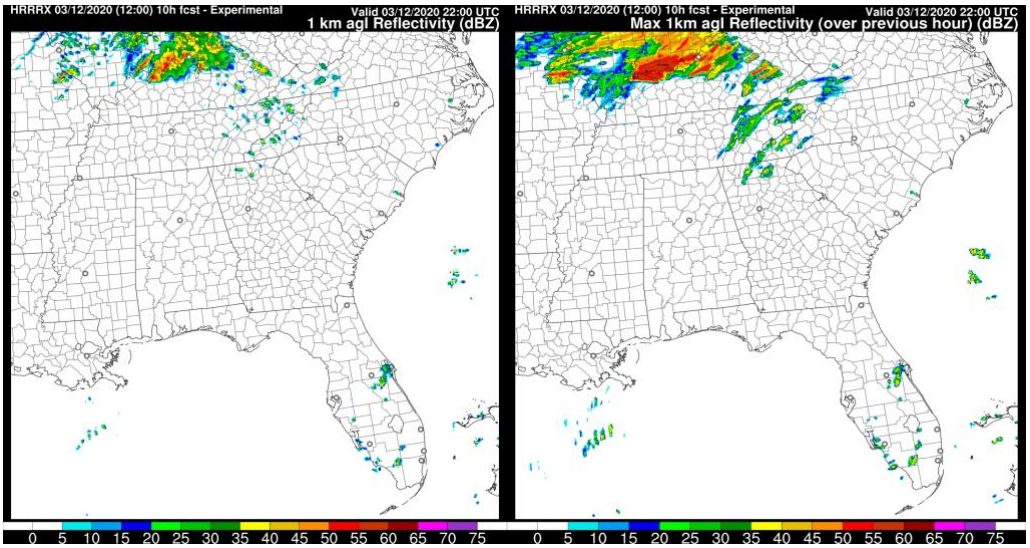

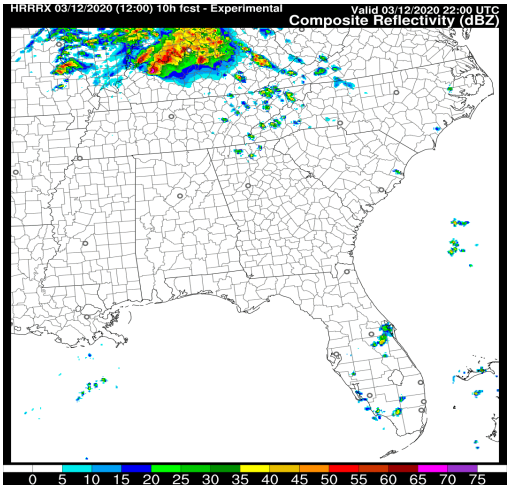

Fig. 33. Reflectivity fields. **(Units - dBZ).** All are 10-h forecasts from the 12z/12 March 2020 HRRRv4 valid 22z/12 March. **Top row** displays two types of reflectivity at the 1-km AGL level, (upper left) instantaneous reflectivity at the forecast time (here 22z) and (upper right) maximum reflectivity over the previous hour (1-h period ending at 22z). **Middle row:** composite reflectivity. In the **bottom row:** two types of reflectivity interpolated to the -10ºC level are displayed.

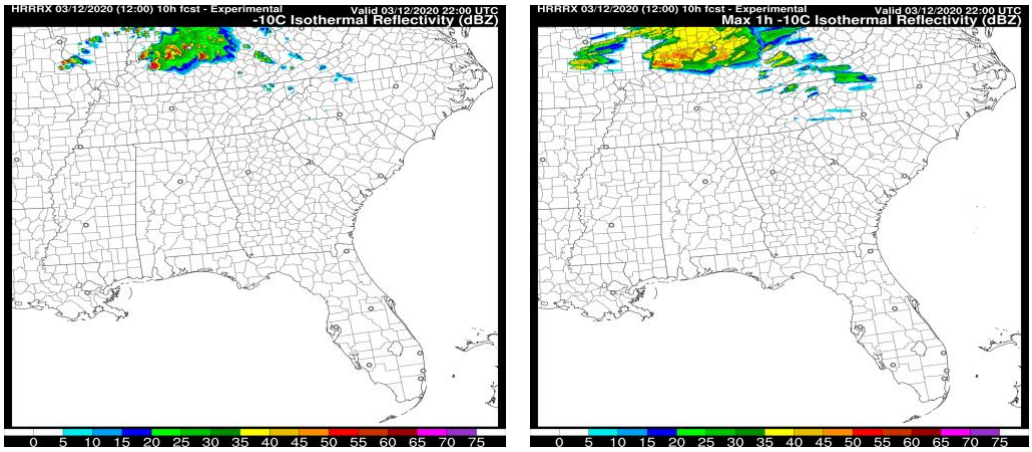

ii. Lightning diagnostic (for convection-allowing model output with explicit microphysics)

Hourly maximum lightning threat is a measure of total lightning (cloud-to-ground and in-cloud). It is calculated for each model column based on the vertically integrated ice (cloud ice, snow, graupel) and the vertical graupel flux (vertical motion and graupel) (McCaul et al., 2009). The units are flashes per square km every 5 minutes; Fig. 34. It attempts to capture both lower frequency, broad anvil lightning and higher frequency lightning near updrafts. The McCaul scheme consists of two algorithms ("Threat 1" and "Threat 2") that are combined to produce a blended lightning, Threat 3.

Threat 1: Graupel Flux at -15ºC. This is the product of q_g and w, where q_g is the predicted mixing ratio of graupel, and w is the vertical velocity, both interpolated to the level where the temperature is -15ºC. This can be looked at as an estimate of charge separation produced in an updraft. This is done for each horizontal grid point, to produce a horizontal map of Threat 1.

Threat 2: Vertical Ice Integral. This is the vertical integral of all ice hydrometeors at each horizontal grid point. The ice hydrometeors (from the Thompson scheme) are q_i (cloud ice), q_s (snow), and q_g (graupel). This threat diagnostic is an attempt to capture the lightning threat from thunderstorm anvils, where vertical motions are weak, but a considerable concentration of charged ice particles may be present aloft.

Threat 3 = a * Threat 1 + b * Threat 2, where a and b are empirically determined weights.

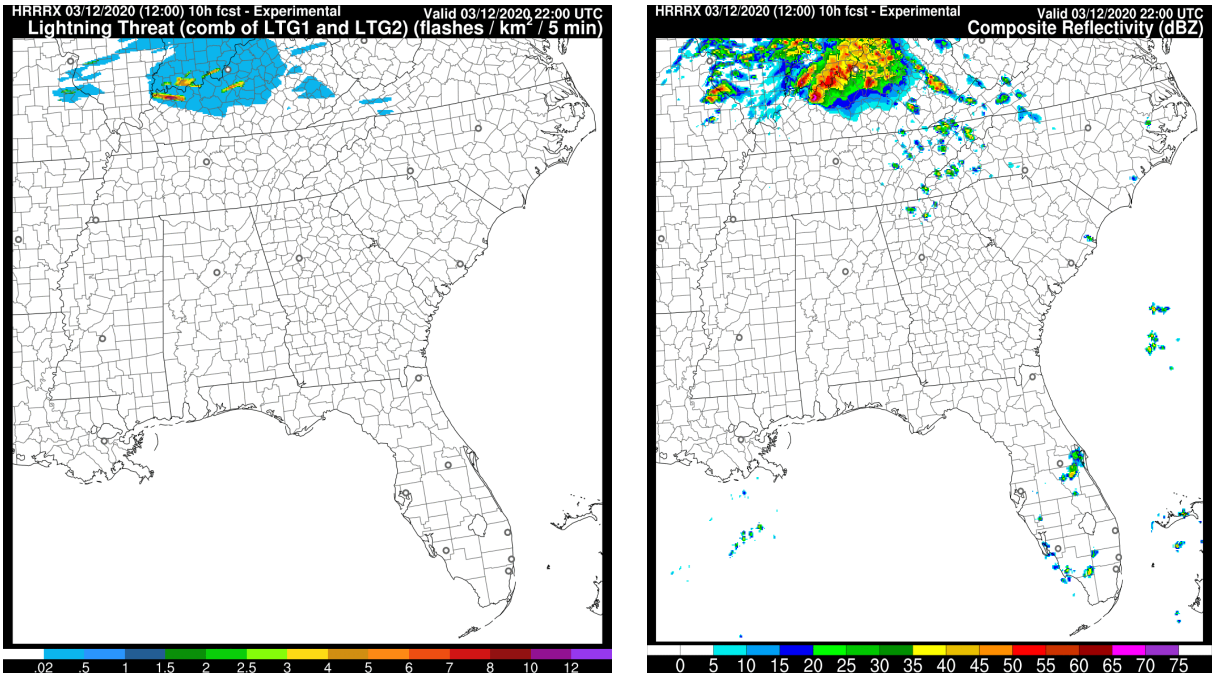

Fig. 34. Lightning Threat using McCaul diagnostic. 10-h forecast valid at 22z/12 Mar 2020 from the 12z/12 Mar HRRRv4, compared to composite reflectivity from the same forecast on right.

iii. Updraft helicity

Hourly maximum and minimum updraft helicity (UH) are calculated as hourly maxima or minima valid at the end of each hour. UH is derived from upward vertical velocity and vertical vorticity for a given vertical layer; HRRR maximum UH (cyclonic) and minimum UH (anticyclonic) are diagnosed between 0 and 2 km, 0 and 3 km, 2 and 5 km, and 1 and 6 km AGL. In cases where the lower boundary is at 0 km AGL, the 10-m wind field is used as the wind at the lower boundary. UH indicates updraft rotation in forecasted convection, which can imply a threat for tornadoes but does not explicitly predict tornadoes. UH maxima identify cyclonic rotation, while minima identify anticyclonic rotation. Since UH depends partially on updraft strength, it can be small in low CAPE, highly sheared environments. It does not discriminate between elevated and surface-based convection.

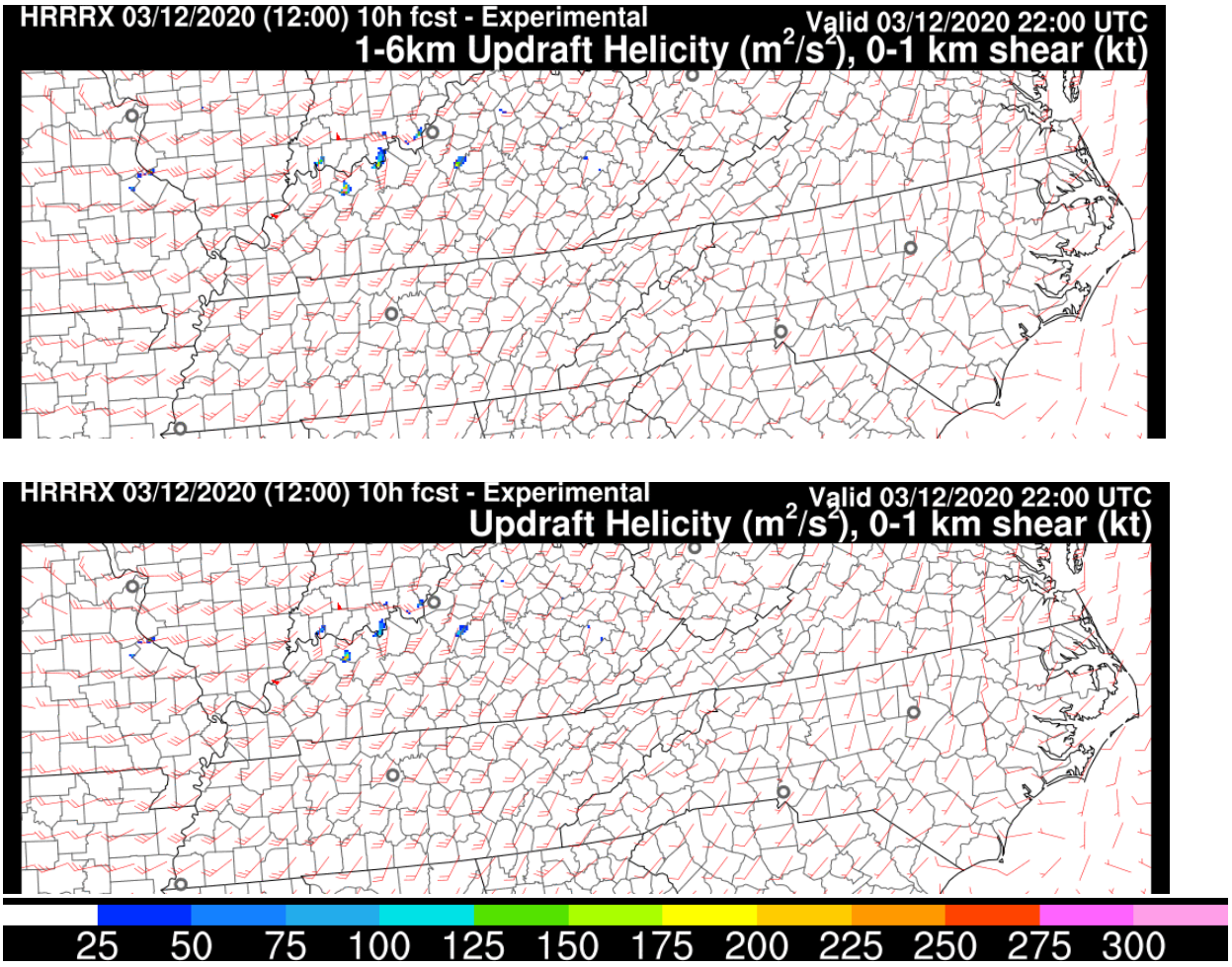

Fig. 35. Updraft helicity (UH - <u>Instantaneous</u> values, in m^2s^{-2}). Shown here from the HRRR website for two levels, displayed with 0-1 km vertical shear vector (wind barb). Top image is for the 1-6 km UH and the bottom image for the 2-5 km UH. Both are 10-h forecasts valid at 22z/12 Mar from the 12z/12 Mar HRRRv4 for a severe weather event.

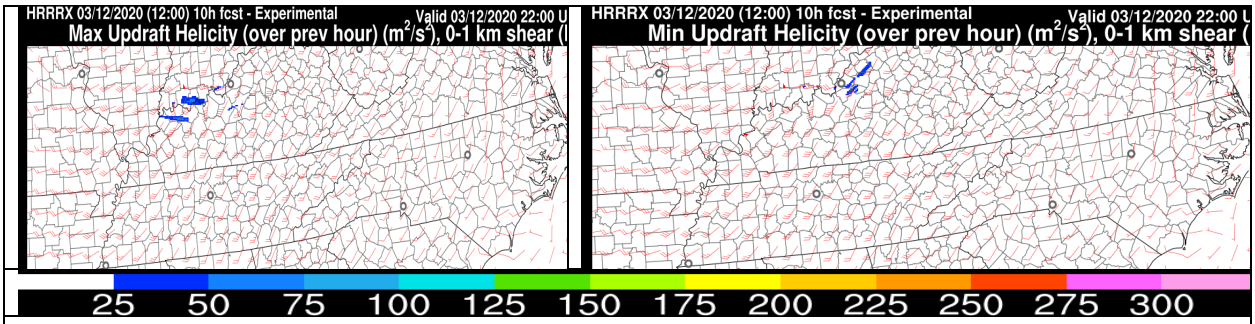

Fig. 36. Maximum/minimum 0-1 km updraft helicity (m^2s^{-2}) over previous 1-h period. Also shown - 0-1 km vertical shear vector (wind barb). Maximum UH values are calculated for previous hour to show UH tracks for cyclonically rotating model storms (top - "*right-movers*") and minimum UH over the previous hour to show UH tracks for *anticyclonically* rotating model storms (lower - "*left-movers*"). For this case, UH is shown for the 0-1 km layer. For 10-h forecasts valid at 22z/12 Mar for the 0-1 km shear and for the 1-h period ending at 22z for the UH, from the 12z/12 Mar HRRRv4.

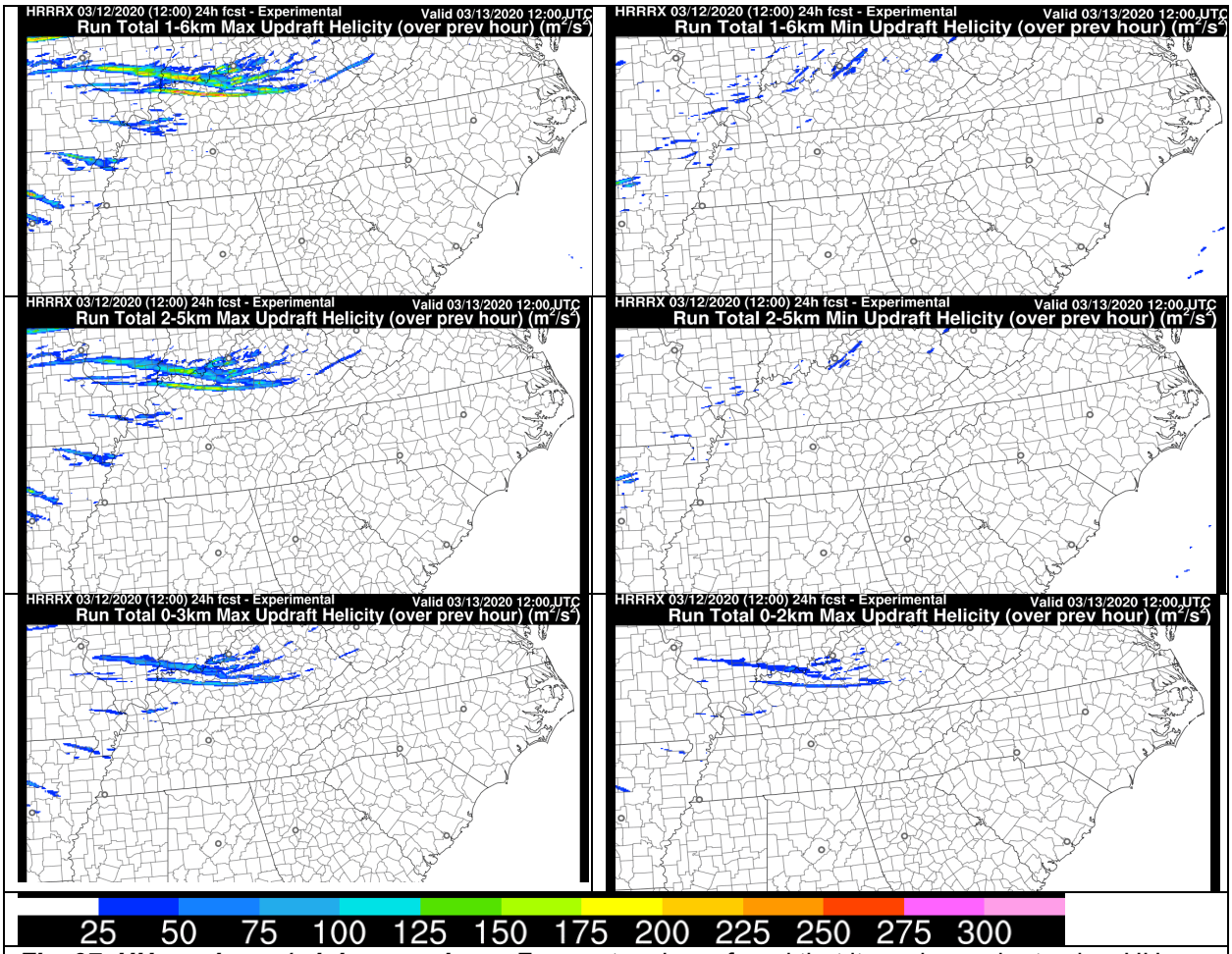

Fig. 37. UH maximum/minimum values. Forecasters have found that it can be easier to view UH values as tracks over a period of time, which can be useful since supercells can last for many hours, both in the model and the real world. UH fields are provided for these layers: 1-6 km, 2-5 km, 0-3 km and 0-2 km AGL. The forecasts shown above are all 24-h UH tracks ending at 12z/13 March for these various levels for both max and min UH values, all from the 12z/12 March 2020 HRRRv4. There were several supercells on this day producing severe weather including a few tornadoes.

iv. Vertical velocity

Hourly maximum updraft velocity / downdraft velocities are the maximum upward/downward vertical velocities (m s^{-1}) between the surface and 100 hPa (Fig. 38). They do not indicate where in the vertical column the maximum occurred or when during the hour. Hourly mean vertical velocity is the average vertical velocity (m s^{-1}) between sigma level 0.8 and 0.5 (approximately 800 hPa and 470 hPa) and averaged over the 1-h period.

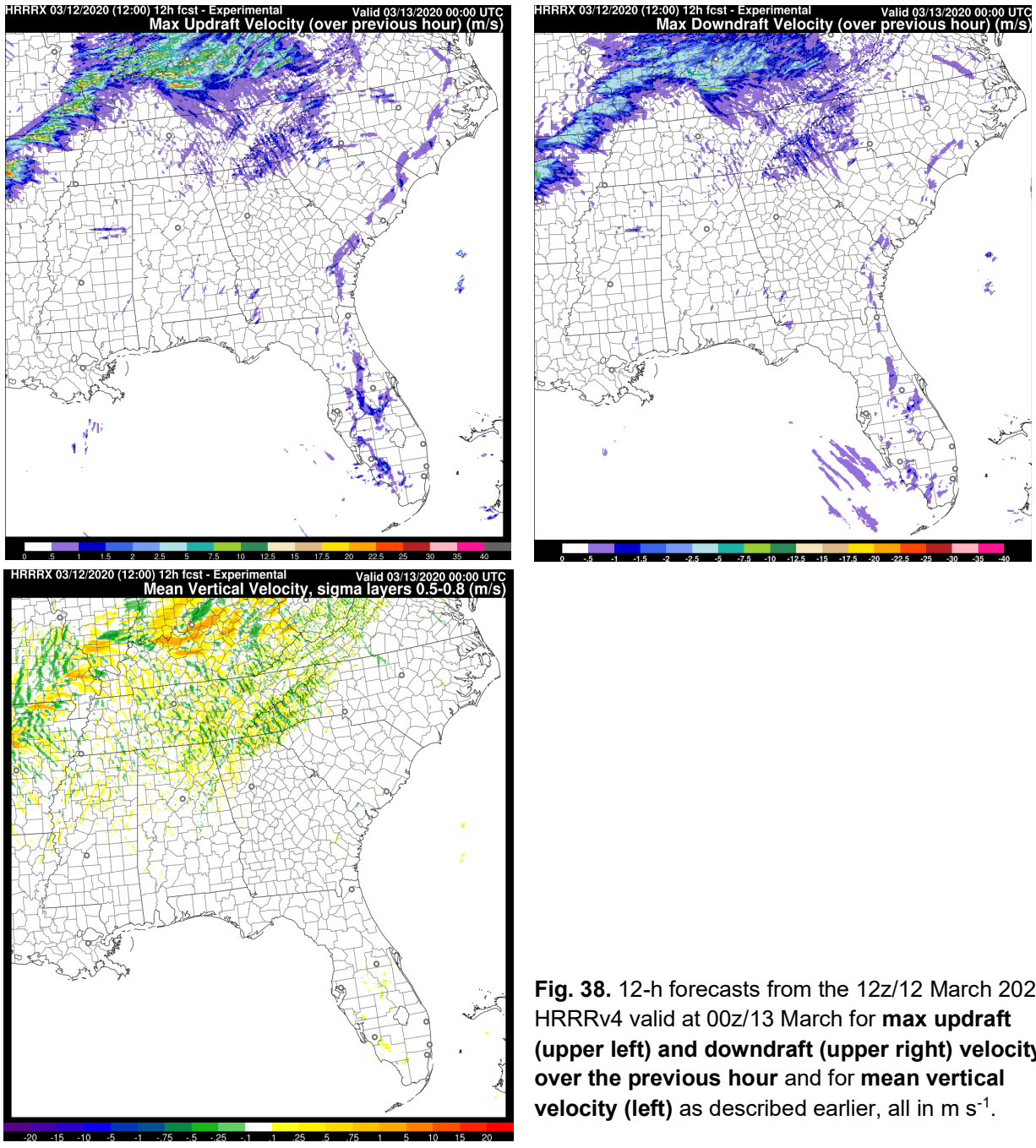

Fig. 38. 12-h forecasts from the 12z/12 March 2020 HRRRv4 valid at 00z/13 March for **max updraft (upper left) and downdraft (upper right) velocity over the previous hour** and for **mean vertical velocity (left)** as described earlier, all in m s^{-1}.

v. Vertical vorticity

Vertical vorticity is another diagnostic measuring the strength of low-level rotation within or outside of the convection and does not account for updraft strength. Hourly maximum vertical vorticity is diagnosed in the HRRR for the 0-1 km layer and the 0-2 km layer (Fig. 39).

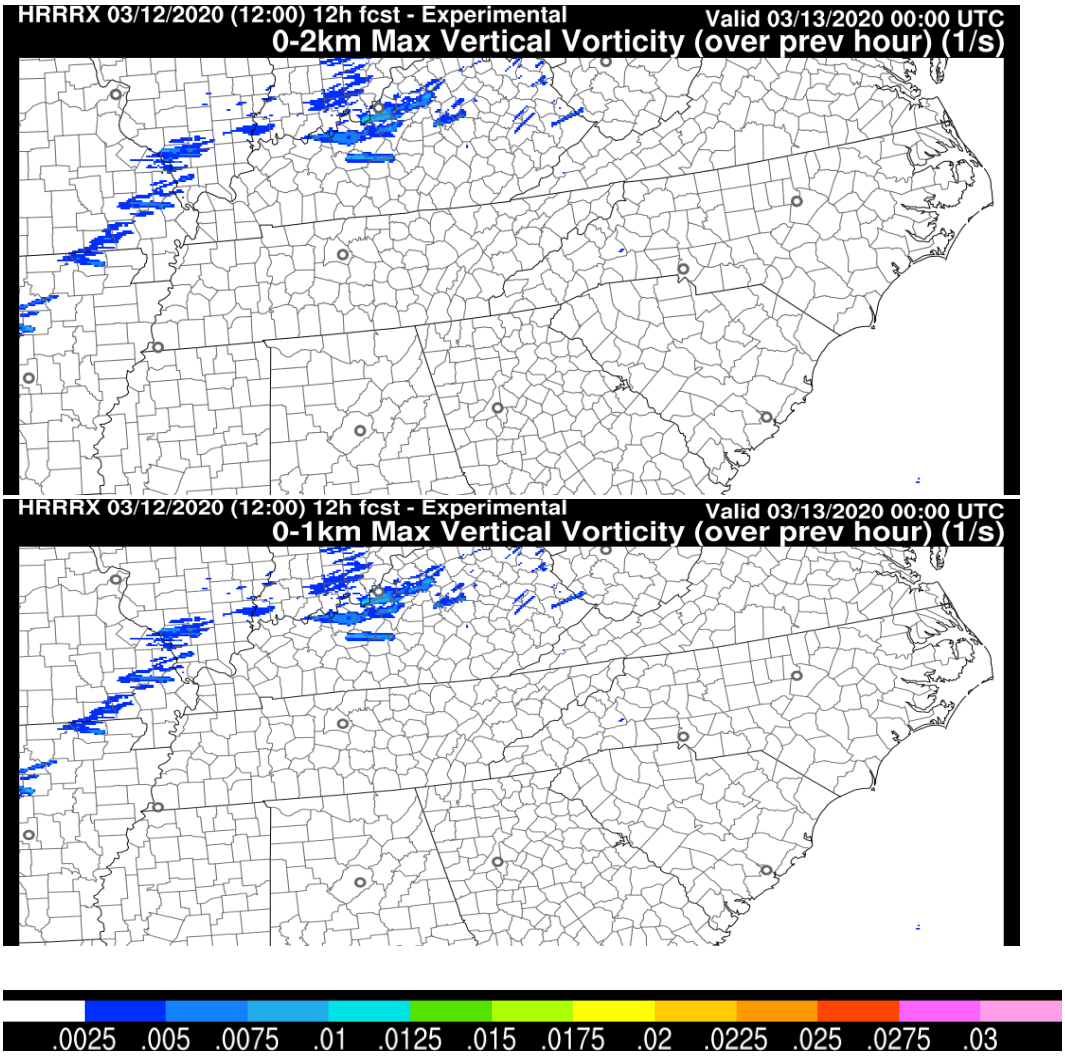

Fig. 39. Vertical vorticity (s^{-1}). For the 0-2 km (AGL) layer (top) and 0-1 km layer (bottom), 12h forecast valid at 00z/13 March from the 12z/12 March 2020 HRRRv4.

vi. Vertically integrated liquid (VIL)

VIL is calculated from reflectivity to produce an estimate of *vertically integrated liquid* in kg m^{-2}. This output VIL is not the same as the vertical cloud liquid water path. For an average vertical profile within a convective storm, 12 kg m^{-2} VIL is very roughly equivalent to a 50 dBZ reflectivity although VIL is, by definition, a vertically integrated quantity. Two different VIL diagnostics are described below.

VIL (hydrometeor-based diagnostic, provided in HRRR/RAP but not in RRFSv1): Uses a vertical summation of three microphysics hydrometeors including rain, snow, and graupel mixing ratios (no cloud water or cloud ice) in each model column. This diagnostic approach assumes a linear relationship between contributions from different hydrometeors even though the actual relationship is nonlinear.

VIL (radar-based diagnostic): Involves computing model radar reflectivity (*Z*) at all levels in each model column from the precipitation hydrometeors (using both mixing ratios and number concentrations) and then using the familiar mapping of reflectivity factor to VIL (vertical integral of 3.44 * $Z^{4/7}$, see Greene and Clark 1972) to produce a field called "Radar VIL." This method is designed to better approximate "observed" VIL from WSR-88D (and other) radars. The radar VIL diagnostic tends to produce lower values when compared to the hydrometeor VIL field, especially around the periphery of more intense moist convective updrafts.

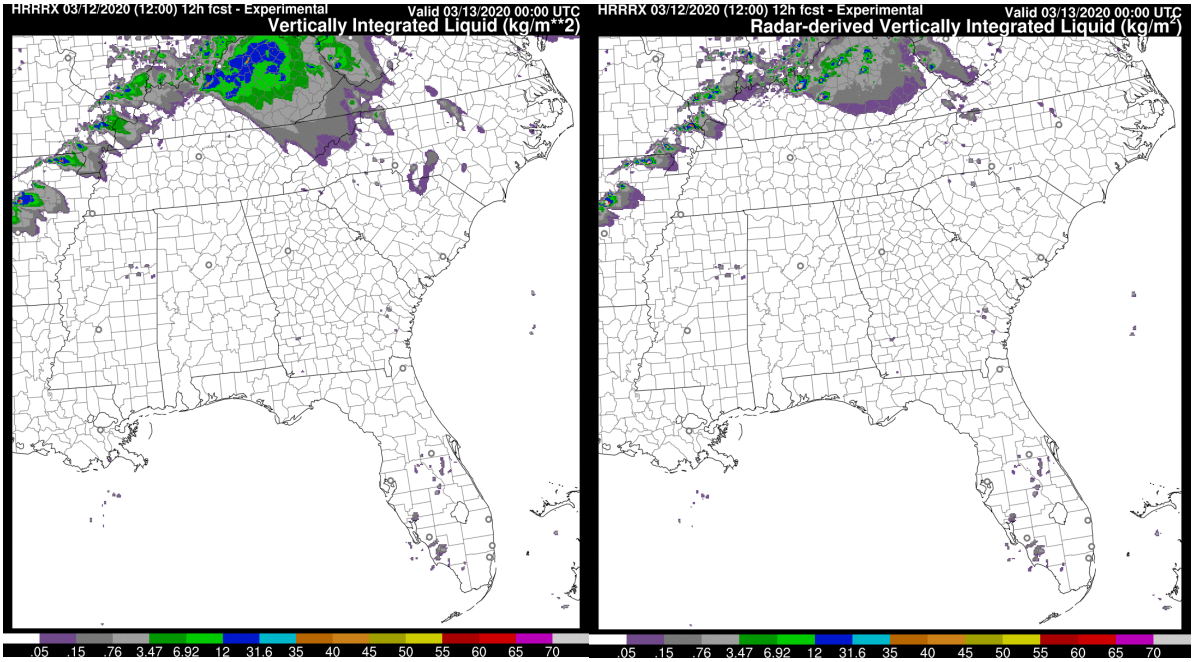

Fig. 40. Vertically integrated liquid. Hydrometeor-based diagnostic (left) and radar-based diagnostic (right). Units - kg m^{-2}. Both are 12-h forecasts valid at 00z/13 March from the 12z/12 March 2020 HRRRv4.

vii. Echo-top level

This field is the maximum height (in m above sea level) at which reflectivity exceeds 18 dBZ (Fig. 41) in a column and is calculated from a vertical profile of reflectivity.

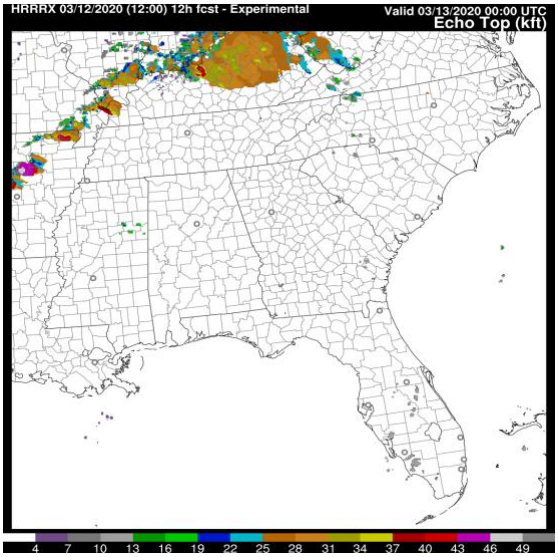

Fig. 41. Echo top. 12-h forecast from the 12z/12 March 2020 HRRRv4 valid at 00z/13 March. Units shown in graphic - kft ASL.

viii. Hourly maximum/minimum fields

Maximum hourly fields contain the maximum value across every model time-step (20 seconds in HRRR model, 36 seconds in RRFSv1) at each grid point during that hour. Care must be taken to interpret these fields because one cannot tell when during the hour a feature occurred. Spatial structure could imply one feature moving or multiple features. Hourly maxima can be used to help identify temporal and spatial phase errors in the forecast, and to help infer if features are transient or longer-lived. Hourly maximum fields are provided for the following variables (all of which are described earlier in this section):

- Radar reflectivity at 1 km AGL
- Radar reflectivity at -10ºC
- Lightning threat
- Updraft helicity
- Vertical vorticity
- 10-m wind
- Updraft velocity
- Downdraft velocity

I. Other upper-air diagnostics

i. Tropopause variables

In the RAP and RRFSv1, tropopause pressure is diagnosed in the standard Unipost configuration with a surface-upward search for first occurrence of a 3-layer mean lapse rate less than or equal to a critical lapse rate (2 K km^{-1}) in accordance with WMO definition of the tropopause. Low tropopause regions correspond to upper-level waves and give a quasi-3D way to look at upper-level potential vorticity. They also correspond well to dry (warm) areas in water vapor satellite images, since stratospheric air is very dry. For RAP and RRFSv1, tropopause-level fields are also provided for temperature, potential temperature, and u/v wind components. No tropopause fields are provided for HRRR.

ii. Vertical velocity

Following NCEP Unipost convention, vertical velocity in m/s is converted to omega in Pa/s using the formula *omega = -rho*g*w*, where *rho* is air density and *g* = 9.80665 m s^{-2}. *(The vertical motion is instantaneous (at a given model time step) and is not time-averaged.)*

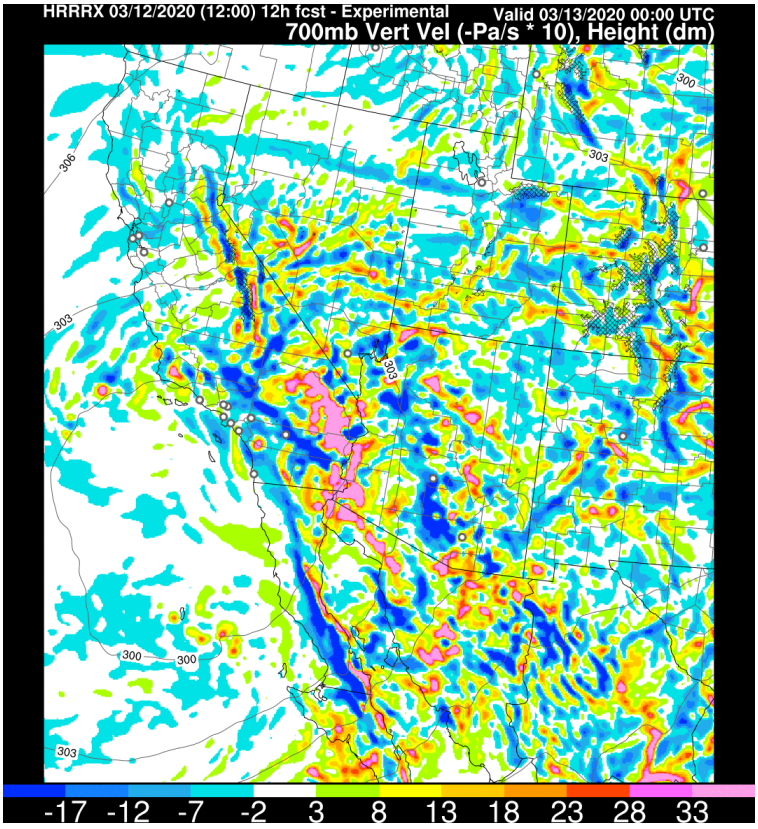

Fig. 42. 700 hPa vertical velocity (-Pa s^{-1}). 12h forecast from the 12z/12 March 2020 HRRRv4 valid at 00z/13 March.

iii. Freezing levels

Two sets of freezing levels are output from RAP/HRRR and RRFS, one searching in the column from the bottom up, and one searching from the top down. Of course, these two sets may be equivalent under many situations, but they may sometimes identify multiple freezing levels (important for aviation). The bottom-up algorithm will return the surface as the freezing level if any of the bottom 3 native levels (up to about 80 m above the surface) are below freezing (per instructions from the NOAA Aviation Weather Center, which uses this product). The top-down freezing level returns the first level at which the temperature goes above freezing searching from the top downward. For both the top-down and bottom-up algorithms, the freezing level is actually interpolated between native levels to estimate the level at which the temperature goes above or below freezing.

iv. Isobaric level vs. native level output for HRRR and RAP and RRFSv1

Fields on the native model levels from HRRR, RAP and RRFSv1 are never horizontally smoothed. By contrast, for HRRR and RAP (but not RRFSv1), isobaric fields are horizontally smoothed for temperature, height, RH, and u/v components of horizontal winds since these fields are often used for horizontal maps. For all 3 models (RRFSv1, HRRR, RAP), for studies of local structure (e.g., orographic, coastal, storm, others), users are advised to use native-level data and not use isobaric data.

J. Smoke-related, wildfire-related and dust diagnostics *(introduced with HRRRv4/RAPv5 and further with RRFS)*

RAPv5 / HRRRv4 in 2020 and continuing with RRFSv1 explicitly predict concentrations of wildfire smoke at each 3-d grid point. Data assimilation using fire radiative power data from

satellites and model effect on radiation from smoke are described by Ahmadov et al (2017) and more recently by Li et al (2025). Smoke-related diagnostic variables, described below, are output for RAPv5, HRRRv4 and RRFSv1. Explicitly predicted dust mixing ratio is also output in RRFSv1. The GRIB2 labeling conventions for smoke and dust related products are provided in Table 4.

Table 4. Atmospheric composition diagnostics from RAPv5/HRRRv4/RRFSv1. Note that the RAPv5/HRRRv4 MASSDEN fields do not have any associated aerosol type or aerosol size, since smoke < 2.5 x 10^{-6} m is the only air quality tracer in those modeling systems.

Variable	**GRIB2 label**	**GRIB2 aerosol type**	**GRIB2 aerosol size**	**Units**	**In RAPv5 and HRRRv4?**	**In RRFSv1?**
Inst. near-sfc smoke	MASSDEN	Particulate organic matter dry	<2.5 x 10^{-6} m	kg m^{-3}	Yes	Yes
Inst. near-sfc fine dust	MASSDEN	Dust dry	<2.5 x 10^{-6} m	kg m^{-3}	No	Yes
Inst. near-sfc coarse dust	MASSDEN	Dust dry	>=2.5 x 10^{-6} m, <1 x 10^{-5} m	kg m^{-3}	No	Yes
1-h avg near-sfc PM2.5	MASSDEN	Total aerosol	<2.5 x 10^{-6} m	kg m^{-3}	No	Yes
1-h avg near-sfc PM10	MASSDEN	Total aerosol	<1 x 10^{-5} m	kg m^{-3}	No	Yes
Inst. vert. integrated smoke	COLMD	Particulate organic matter dry	<2.5 x 10^{-6} m	kg m^{-2}	Yes	Yes
Inst. vert. integrated fine dust	COLMD	Dust dry	<2.5 x 10^{-6} m	kg m^{-2}	No	Yes
Inst. vert. integrated coarse dust	COLMD	Dust dry	>=2.5 x 10^{-6} m, <1 x 10^{-5} m	kg m^{-2}	No	Yes
AOD	AOTK	-	-	-	Yes	Yes
1-h avg HWP	WFIREPOT*	-	-	-	No	Yes

*Some older GRIB2 interrogation tools may not be able to correctly decode the HWP variable and may display the HWP as “var discipline=2 master_table=2 parmcat=4 parm=26“.

i. Near-surface smoke

A near-surface smoke diagnostic is provided from HRRR, RAP, and RRFSv1 models. This variable is simply the explicit smoke concentration on the lowest model level (~8 m AGL at sea level). The smoke concentration is in the GRIB2 files in units of kg m^{-3}, converted to μg m^{-3} (micrograms per cubic meter) for website graphics.

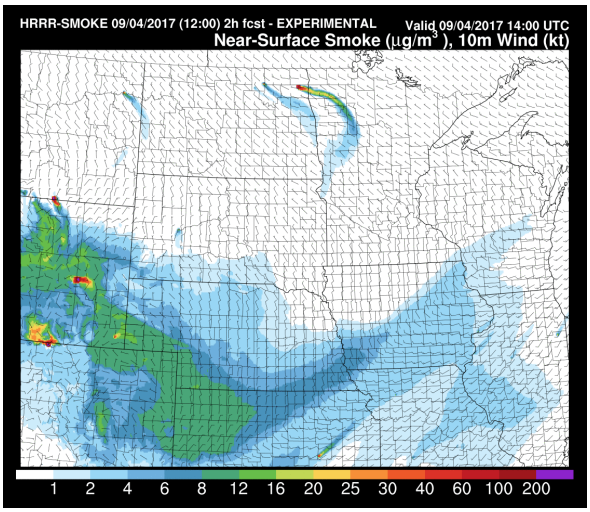

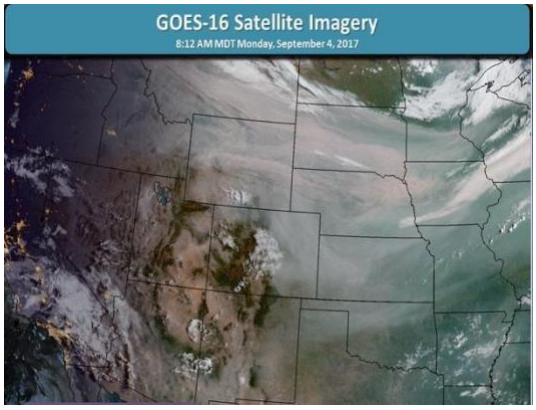

Fig. 43. Near-surface smoke. **(left)** From HRRRv4 (with 10-m wind) for a case of widespread western U.S. fires on 4 September 2017. **GOES-16 GeoColor imagery (right)** shows the observed extent of smoke in the atmosphere, which is likely more comparable to the HRRR forecast product shown below.

ii. Vertically integrated smoke

In addition to the near-surface smoke, a vertically integrated smoke is diagnosed, in which smoke concentrations are summed across all vertical levels. GRIB2 units are in kg m^{-2} (converted to mg m^{-2} for website graphics).

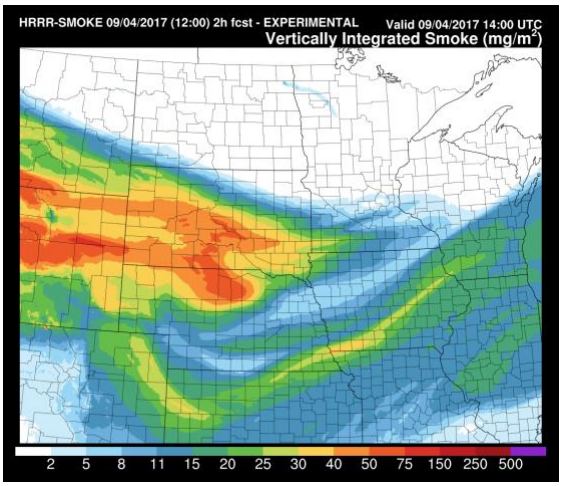

Fig. 44. Vertically integrated smoke. From an early experimental version of HRRRv4 for the same case of widespread western U.S. fires on 4 September 2017.

iii. Aerosol optical depth

A 2-D aerosol optical depth (AOD) for smoke is calculated by vertically integrating the smoke extinction plus that from climatological aerosols. For RRFSv1, AOD also includes dust across all vertical levels. It should be noted that the AOD (see 'AOTK' variable in the GRIB2 files from RAP/HRRR-Smoke or RRFS) does not include the contribution of other aerosols (e.g., urban pollution). AOD is a unitless quantity.

Iv. Hourly Wildfire Potential

A new wildfire potential diagnostic based on near-surface wind gust potential, soil moisture, snow cover, and near-surface water-vapor saturation deficit (James et al. 2025) is now available from RRFSv1 (in GRIB2 output) and also available on the website for HRRRv4. This variable is available hourly and is called the ***Hourly Wildfire Potential*** (HWP). The HWP is intended to reflect hourly changes in fire activity on any ongoing fires based on changes in the weather. Examples of HWP are presented in Fig. 45 for a case from November 2025.

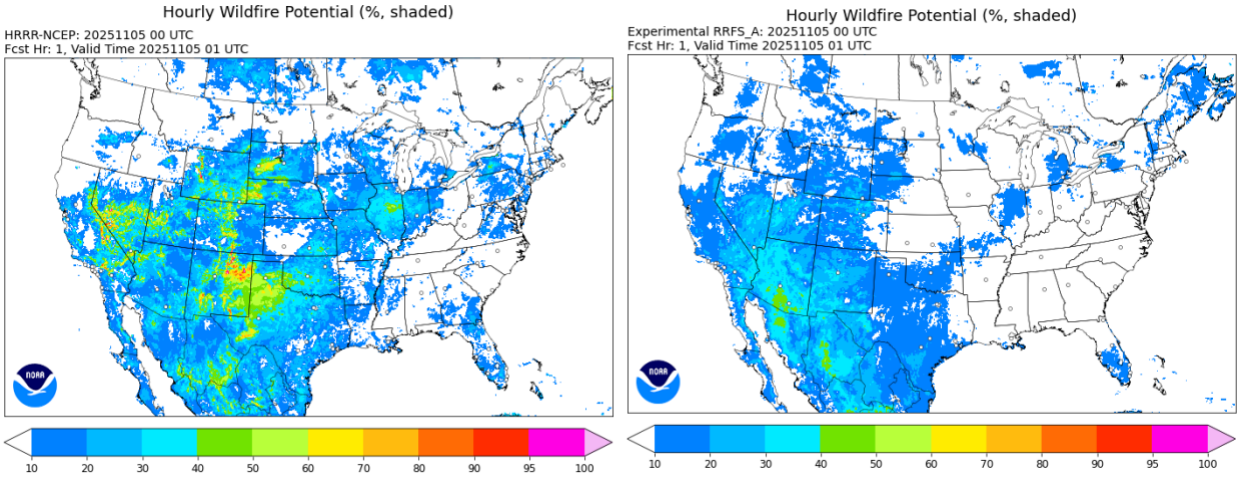

Fig. 45. Hourly Wildfire Potential (HWP). From 1-h forecasts valid at 0100 UTC 5 November 2025 for HRRRv4 (left) and RRFSv1 (right).

v. Near-surface dust and vertically integrated dust.

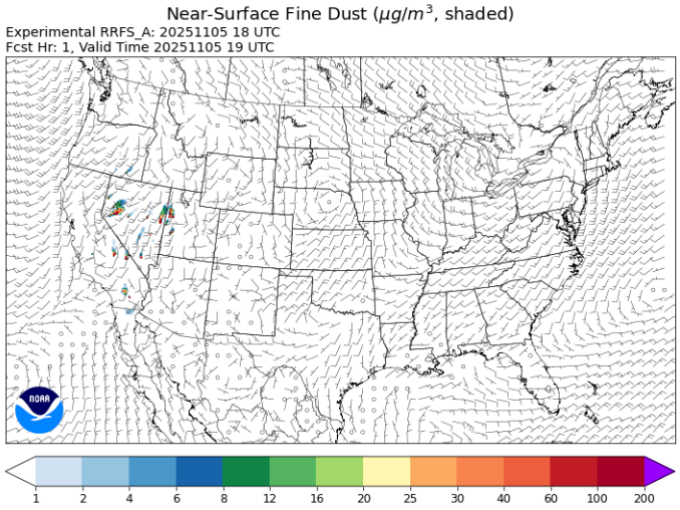

Fig. 46. Near-surface fine-grain dust concentration (ug/m^3). For 1-h RRFSv1 forecast valid at 19 UTC 5 November 2025.

As described above, fine-grain and coarse-grain dust concentrations were added as prognostic variables in RRFSv1 as described in Li et al. (2025). A dust emission function is used in RRFSv1, highly dependent on near-surface wind speed. An example of near-surface (lowest model level, about 10 m AGL) dust concentration is shown in Fig. 46 with some dust evidence over Nevada and Utah. Vertically integrated dust is another output product from RRFSv1, corresponding to the previously described vertically integrated smoke product. Note that, for RRFS, additional diagnostics are provided corresponding to hourly-average PM2.5 (smoke + fine dust) and PM10 (smoke + fine dust + coarse dust; see Table 4). These hourly-average fields allow for more direct comparison with surface regulatory monitors, which are generally provided as an hourly average.

Acknowledgments

The authors thank Shawn Murdzek (GSL, CIRES) for an excellent internal review that greatly improved this document. As cited for the previous diagnostics technical memorandum, many of these diagnostic descriptions resulted from questions from HRRR/RAP/RUC model data users, especially from National Weather Service forecasters, over the years.

4. References

Adams-Selin, R. D., and C. L. Ziegler, **2016**: Forecasting hail using a one-dimensional hail growth model within WRF. *Mon. Wea. Rev,* **144,** 4919-4939. https://doi.org/10.1175/MWR-D-16-0027.1

Ahmadov, R., G. Grell, E.P. James, I. Csiszar, M. Tsidulko, R.B. Pierce, S. McKeen, S.G. Benjamin, C.A. Alexander, G. Pereira, S. Freitas, M. Goldberg, **2017**: Using VIIRS Fire Radiative Power data to simulate biomass burning emissions, plume rise and smoke transport in a real-time air quality modeling system. IEEE International Geoscience and Remote Sensing Symposium, New York, 2806-2808. https://ieeexplore.ieee.org/document/8127581

Aligo, E.A., B. Ferrier, and J.R. Carley, **2018**: Modified NAM microphysics for forecasts of deep convective storms. *Mon. Wea. Rev.*, **146**, 4115-4153.

Benjamin, S. G., and P. A. Miller, **1990**: An alternative sea level pressure reduction and a statistical comparison of geostrophic wind estimates with observed surface winds. *Mon. Wea. Rev.,* **118,** 2099-2116. https://doi.org/10.1175/1520-0493(1990)118<2099:AASLPR>2.0.CO;2.

Benjamin, S. G., D. Dévényi, S. S. Weygandt, K. J. Brundage, J. M. Brown, G. A. Grell, D. Kim, B. E. Schwartz, T. G. Smirnova, T. L. Smith, and G. S. Manikin, **2004**: An hourly assimilation/forecast cycle: The RUC. *Mon. Wea. Rev*., **132**, 495-518. https://doi.org/10.1175/1520-0493(2004)132<0495:AHACTR>2.0.CO;2.

Benjamin, S. G., S. S. Weygandt, J. M. Brown, M. Hu, C. R. Alexander, T. G. Smirnova, J. B. Olson, E. P. James, D. C. Dowell, G. A. Grell, H. Lin, S. E. Peckham, T. L. Smith, W. R. Moninger, J. S. Kenyon, and G. S. Manikin, **2016a**: A North American hourly assimilation and model forecast cycle: The Rapid Refresh. *Mon. Wea. Rev.,* **144,** 1669-1694. http://dx.doi.org/10.1175/MWRF-D-15-0242.1.

Benjamin, S. G., J. M. Brown, and T. G. Smirnova, **2016b**: Explicit precipitation-type diagnosis from a model using mixed-phase bulk cloud-precipitation microphysics parameterization. *Wea. Forecasting,* **31,** 609-619. https://doi.org/10.1175/WAF-D-15-0136.1.

Benjamin, S.G., E.P. James, J.M. Brown, E.J. Szoke, J.S. Kenyon, R. Ahmadov, D.D. Turner, **2021a**, Diagnostic fields developed for hourly updated NOAA weather models. NOAA Tech. Memo. OAR GSL-66. https://doi.org/10.25923/f7b4-rx42 .

Benjamin, S.G., E.P. James, M. Hu, C.R. Alexander, T.T. Ladwig, J.M. Brown, S.S. Weygandt, D.D. Turner, P. Minnis, W.L. Smith, Jr., and A.K. Heidinger, **2021b**: Stratiform cloud-hydrometeor assimilation for HRRR and RAP model short-range weather prediction. *Mon. Wea. Rev.*, **149**, https://doi.org/10.1175/MWR-D-20-0319.1.

Benjamin, S.G., T.G. Smirnova, E.P. James, L.-F. Lin, D.D. Turner, S. He, **2022a**: Land-snow data assimilation including a moderately coupled initialization method applied to NWP. *J. Hydromet.*, **23**. https://doi.org/10.1175/JHM-D-21-0198.1

Benjamin, S.G., T.G. Smirnova, E.P. James, E.J. Anderson, A. Fujisaki-Manome, J.G.W. Kelley, G.E. Mann, A.D. Gronewald, P. Chu, S.G.T. Kelley, **2022b**: Inland lake temperature initialization via coupled cycling with atmospheric data assimilation. *Geo. Model. Dev*., **15**, 6659-6676. https://doi.org/10.5194/gmd-15-6659-2022

Benjamin, S.G., E.P. James, D.D. Turner, K.A. Balmes, J. Sedlar, K.O. Lantz, A. Jensen, L.D. Riihimaki, and J.A. Augustine, **2025**: Excessive downward shortwave radiation in the HRRR and RAP weather models and testing strategies for improvements. *Mon. Wea. Rev*., **153**, 2279-2293, https://doi.org/10.1175/MWR-D-25-0094.1

Bunkers, M. J., B. A. Klimowski, J. W. Zeitler, R. L. Thompson, and M. L. Weisman, **2000**: Predicting supercell motion using a new hodograph technique. *Wea. Forecasting,* **15,** 61-79. https://doi.org/10.1175/1520-0434(2000)015<0061:PSMUAN>2.0.CO;2.

Carley, J., C. Alexander, L. Wicker, C. Jablonowski, A. Clark, J. Nelson, I. Jirak, and K.

Viner, **2023**: Mitigation efforts to address Rapid Refresh Forecast System (RRFS) v1 dynamical core performance issues and recommendations for RRFS v2. NOAA NCEP Office Note 516. https://doi.org/10.25923/ccgj-7140 .

Corrie, T.D., B. Geerts, T.G. Smirnova, S.G. Benjamin, M. Charnick, M. Brothers, S. He, Z.J. Lego, and E.P. James, **2024**: Representation of blowing snow and associated visibility reduction in an operational high-resolution weather model. *Wea Forecasting,* **39**, 1319-1334. https://doi.org/10.1175/WAF-D-23-0195.1

Dowell, D. C., and Coauthors, **2022**: The High-Resolution Rapid Refresh (HRRR): An hourly updating convection-allowing forecast model. Part I: Motivation and system description. *Wea. Forecasting*, **37**, 1371–1395, https://doi.org/10.1175/WAF-D-21-0151.1

Fujisaki-Manome, A., G.E. Mann, E.J. Anderson, P.Y. Chu, L.E. Fitzpatrick, S.G. Benjamin, E.P. James, T.G. Smirnova, C.R. Alexander, and D.M. Wright, **2020**: Improvements to lake-effect snow forecasts using a one-way air-lake model coupling approach. *J. Hydromet*. DOI:10.1175/JHM-D-20-0079.1.

Greene, D.R. and R.A. Clark, **1972**: Vertically integrated liquid water -- A new analysis tool. *Mon. Wea. Rev.,* **100,** 548-552. *https://doi.org/10.1175/1520-0493(1972)100<0548:VILWNA>2.3.CO;2*

Grell, G. A., and D. Dévényi, **2002**: A generalized approach to parameterizing convection combining ensemble and data assimilation techniques. *Geophys. Res. Letters,* **29 (14),** 38-1-38-4. https://doi.org/10.1029/2002GL015311.

Grell, G. A. and S. R. Freitas, **2014**: A scale and aerosol aware stochastic convective parameterization for weather and air quality modeling. *Atmos. Chem. Phys.,* **14,** 5233-5250. https://doi.org/10.5194/acp-14-5233-2014.

Griffin, S. M., J. A. Otkin, C. M. Rozoff, J. M. Sieglaff, L. M. Cronce, C. R. Alexander, T. L. Jensen, and J. K. Wolff, **2017**: Seasonal analysis of cloud objects in the High-Resolution Rapid Refresh (HRRR) model using object-based verification. *J. Appl. Meteor. Climatol.,* **56,** 2317-2334. https://doi.org/10.1175/JAMC-D-17-0004.1.

Han, Y., P. van Delst, Q. Liu, F. Weng, B. Yan, R. Treason, and J. Derber, **2006**: JCSDA Community Radiative Transfer Model (CRTM)--Version 1. NOAA Tech. Re. NESDIS 122, 33 pp.

James, E.P., and Coauthors, **2022**: The High-Resolution Rapid Refresh (HRRR): An Hourly Updating Convection-Allowing Forecast Model. Part II: Forecast Performance, *Wea. Forecasting*, **37**, 1397-1417, https://doi.org/10.1175/WAF-D-21-0130.1

James, E., and Coauthors, **2025**: An Hourly Wildfire Potential index for predicting subdaily fire activity based on rapidly updating convection-allowing model forecasts. *Wea. Forecasting*, **40**, 1805-1822. https://doi.org/10.1175/WAF-D-24-0068.1

Koren, V., J. Schaake, K. Mitchell, Q.-Y. Duan, F. Chen, J. M. Baker, **1999**: A parameterization of snowpack and frozen ground intended for NCEP weather and climate models. *J.*

Geophys. Res., **104,** 19569-19585. https://doi.org/10.1029/1999JD900232.

Li, H., R. Ahmadov, J. Romero-Alvarez, G.A. Grell, J. Olson, J. Schnell, E. James, S. Trahan, M. Hu, S. Bhimireddy, **2025**: Enhancing aerosol direct feedback for numerical weather prediction in NOAA's Rapid Refresh Forecast System – Smoke and Dust (RRFS-SD v1). *Geoph. Res. Let*, **52**. https://doi.org/10.1029/2025GL115384

McCaul, E. W., Jr., S. J. Goodman, K. M. LaCasse, and D. J. Cecil, **2009**: Forecasting lightning Thread using cloud-resolving model simulations. *Wea. Forecasting,* **24,** 709-729. https://doi.org/10.1175/2008WAF2222152.1.

Mesinger, F., and R. E. Treadon, **1995**: "Horizontal" reduction of pressure to sea level: Comparison against the NMC's Shuell method. *Mon. Wea. Rev.,***123,** 59–68.

NOAA, **2019**: Federal Meteorological Handbook No. 1, Surface Weather Observations and Reports. FCM-HA-2019, Washington, DC, July 2019. Available at https://www.icams-portal.gov/resources/ofcm/fmh/FMH1/fmh1_2019.pdf. Last accessed 9 June 2025.

Olson, J. B., J. S. Kenyon, and co-authors, **2019a**: Improving wind energy forecasting through numerical weather prediction model development. *Bull. Amer. Meteor. Soc.,* **100**, 2201-2220. https://doi.org/10.1175/BAMS-D-18-0040.1.

Olson, J. B., J. S. Kenyon, W. M. Angevine, J. M. Brown, M. Pagowski, and K. Sušelj, **2019b**: A description of the MYNN-EDMF scheme and coupling to other components in WRF-ARW. NOAA Tech. Memo. OAR GSD 61, 37 pp., https://doi.org/10.25923/n9wm-be49 .

Olson, J. B., and co-authors, **2026**: A Description of the MYNN-EDMF Turbulence Scheme. NOAA Tech. Memo. OAR GSL-77. https://doi.org/10.25923/rahr-sj70

Otkin, J. A., D. J. Posselt, E. R. Olson, H.-L. Huang, J. E. Davies, J. Li, and C. S. Velden, **2007**: Mesoscale numerical weather prediction models used in support of infrared hyper-Spectral measurements simulation and product algorithm development. *J. Atmos. Oceanic Technol.,* **24,** 585-601. https://doi.org/10.1175/JTECH1994.1.

Pauley, P.M., **1998**: An example of uncertainty in sea level pressure reduction. *Wea. Forecasting*, **13**, 833-850. https://doi.org/10.1175/1520-0434(1998)013<0833:AEOUIS>2.0.CO;2

Peckham, S. E., T. G. Smirnova, S. G. Benjamin, J. M. Brown, and J. S. Kenyon, **2016**: Implementation of a digital filter initialization in the WRF model and its application in the Rapid Refresh. *Mon. Wea. Rev.,* **144,** 99-106. https://doi.org/10.1175/MWR-D-15-0219.1.

Pletcher, M.D., P. G. Veals, R. J. Chase, S. D. Hilberg, N. Newman, A. A. Rosenow, and W. J. Steenburgh, **2026**: Snow-to-liquid ratio prediction over the contiguous United States using machine learning. *Wea. Forecasting*. https://doi.org/10.1175/WAF-D-25-0124.1.

Pondeca, M.S.F.V. de, G.S. Manikin, G. DiMego, S.G. Benjamin, D.F. Parrish, R.J. Purser, W.-S. Wu, J. Horel, Y. Lin, R.M. Aune, D. Keyser, L. Anderson, B. Colman, G. Mann, and J. Vavra, **2011**: The Real-Time Mesoscale Analysis at NOAA's National Centers for

Environmental Prediction: Current Status and Development. *Wea. Forecasting*, **26**, 593-612.

Smirnova, T.G., J.M. Brown, and S.G. Benjamin, **1997**: Performance of different soil model configurations in simulating ground surface temperature and surface fluxes. *Mon. Wea. Rev*., **125**, 1870-1884.

Smirnova, T. G., J. M. Brown, S. G. Benjamin, and J. S. Kenyon, **2016**: Modifications to the Rapid Update Cycle Land Surface Model (RUC LSM) available in the Weather Research and Forecasting (WRF) model. *Mon. Wea. Rev.,* **144,** 1851-1865. https://doi.org/10.1175/MWR-D-15-0198.1.

Smirnova, T.G. and S.G. Benjamin, **2025**: Advancements in the RUC land-surface model for use in the next-generation high-resolution weather prediction models. NOAA Tech. Memo. OAR GSL-73. https://doi.org/10.25923/55x8-cy36

Stoelinga, M. T., and T. T. Warner, **1999**: Nonhydrostatic, mesobeta-scale model simulations of cloud ceiling and visibility for an east coast winter precipitation event. *J. Appl. Meteor.,* **38,** 385-404. https://doi.org/10.1175/1520-0450(1999)038<0385:NMSMSO>2.0.CO;2.

Thompson, G., P. R. Field, R. M. Rasmussen, and W. D. Hall, **2008**: Explicit forecasts of winter precipitation using an improved bulk microphysics scheme. Part II: Implementation of a new snow parameterization. *Mon. Wea. Rev.,* **136,** 5095-5115. https://doi.org/10.1175/2008MWR2387.1.

Thompson, G., and T. Eidhammer, **2014**: A study of aerosol impacts on clouds and precipitation development in a large winter cyclone. *J. Atmos. Sci***., 71**, 3636-3658. https://doi.org/10.1175/JAS-D-13-0305.1.

Toy, M.D, J.B. Olson, F. Yang, B. Yang, and S.-Y. Hong, **2025**: A description of the Unified Gravity Wave Drag Package. NOAA Tech Memo OAR GSL-74. https://doi.org/10.25923/v2kx-8e10

Trahan, S., T.G. Smirnova, S.G. Benjamin, and J.S. Kenyon, **2025**: Implementation and demonstration of the CLM lake model in the NOAA Unified Forecasting System (UFS). NOAA Tech Memo. OAR GSL-75. https://doi.org/10.25923/8srx-pm39